Long short term memory networks for predicting resilient Modulus of stabilized base material subject to wet-dry cycles

Mohammad A Al-Zubi, Mahmood Ahmad, Shahriar Abdullah, Beenish Jehan Khan, Wajeeha Qamar, Gamil M S Abdullah, Roberto Alonso González-Lezcano, Sonjoy Paul, N S Abd El-Gawaad, Tariq Ouahbi, et al.

scientific reports

Check for updates

OPEN

Long short term memory networks for predicting resilient Modulus of stabilized base material subject to wet-dry cycles

Mohammad A. Al-Zubi[1], Mahmood Ahmad[2,3,11]✉, Shahriar Abdullah[4], Beenish Jehan Khan[5], Wajeeha Qamar[6], Gamil M. S. Abdullah[7], Roberto Alonso González-Lezcano[8], Sonjoy Paul[4], N. S. Abd EL-Gawaad[9], Tariq Ouahbi[10] & Muhammad Kashif[3]

The resilient modulus (M_R) of different pavement materials is one of the most important input parameters for the mechanistic-empirical pavement design approach. The dynamic triaxial test is the most often used method for evaluating the M_R, although it is expensive, time-consuming, and requires specialized lab facilities. The purpose of this study is to establish a new model based on Long Short-Term Memory (LSTM) networks for predicting the M_R of stabilized base materials with various additives during wet-dry cycles (WDC). A laboratory dataset of 704 records has been used using input parameters, including WDC, ratio of calcium oxide to silica, alumina, and ferric oxide compound, Maximum dry density to the optimal moisture content ratio (DMR), deviator stress (σ_d), and confining stress (σ_3). The results demonstrate that the LSTM technique is very accurate, with coefficients of determination of 0.995 and 0.980 for the training and testing datasets, respectively. The LSTM model outperforms other developed models, such as support vector regression and least squares approaches, in the literature. A sensitivity analysis study has determined that the DMR parameter is the most significant factor, while the σ_d parameter is the least significant factor in predicting the M_R of the stabilized base material under WDC. Furthermore, the SHapley Additive exPlanations approach is employed to elucidate the optimal model and examine the impact of its features on the final result.

Keywords Resilient modulus, Pavements, Stabilized base, Wet-dry cycles, Long short-term memory networks, Graphical user interface

For rigid and flexible pavements, the stabilized aggregate bases are substantial parts of pavement structures, providing structural support and durability. Stabilized aggregate bases are prepared from aggregates, water, and stabilizing additives like cement, lime, fly ash, or asphalt emulsion By adding the stabilizing agents it can enhance the properties of base materials such as the strength, stiffness, and resistance to moisture damage[1]. The stiffness of a soil or pavement layer during repeated loading and unloading situations are defined by Resilient modulus (M_R)[2]. The M_R is utilized to construct flexible pavements that deform elastically under traffic loads[3]. The M_R is also used to assess the performance and durability of stabilized aggregate bases when subjected to Wet-Dry cycles (WDC)[4]. The M_R, which defined subgrade soil stiffness, was incorporated into the pavement design guide of the American Association of State Highway and Transportation Officials (AASHTO) in 1993[5]. Since then,

[1]Department of Mechanical Engineering, Hijjawai Faculty for Engineering, Yarmouk University, Irbid 21163, Jordan. [2]Institute of Energy Infrastructure, Universiti Tenaga Nasional, Kajang 43000, Malaysia. [3]Department of Civil Engineering, University of Engineering and Technology Peshawar (Bannu Campus), Bannu 28100, Pakistan. [4]Department of Civil and Environmental Engineering, Lamar University, Lamar, Texas 77710, USA. [5]Department of Civil Engineering, CECOS University of IT and Emerging Sciences, Peshawar 25000, Pakistan. [6]Department of Civil Engineering, Institute of Engineering and Fertilizer Research, Faisalabad 38000, Pakistan. [7]Department of Civil Engineering, College of Engineering, Najran University, P.O. 1988, Najran, Saudi Arabia. [8]Department of Architecture and Design, Escuela Politécnica Superior, Universidad San Pablo-CEU, CEU Universities, Montepríncipe Campus, Madrid 28668, Spain. [9]Muhayil Asir, Applied College, King Khalid University, Abha 62529, Saudi Arabia. [10]LOMC, UMR 6294 CNRS, Université Le Havre Normandie, Normandie Université, 53 Rue de Prony, Le Havre Cedex 76058, France. [11]Department of Artificial Intelligence, University of Engineering and Technology Peshawar (Bannu Campus), Bannu 28100, Pakistan. ✉email: ahmadm@uetpeshawar.edu.pk; ahmadm@uniten.edu.my

the M_R has been frequently employed to characterize materials in flexible pavement structural design as a vital attribute[6,7]. The M_R of pavement materials is determined using a variety of laboratory experiments that simulate the repeated loading conditions encountered by roads[8–14].

The prevalent environmental factors that can deteriorate the stabilized aggregate bases is the WDC, that is the repeated exposure of the base materials to moisture and drying[15]. Several research studies show that WDC and freeze-thaw cycles (FTC) affect the performance of stabilized aggregate bases. Pavement design standards like AASHTO 1993 and Mechanistic-Empirical Design Guide identify such challenges and their implications[5,16]. According to other research studies and these guidelines, WDC and FTC damage engineering properties and lead to pavement degradation and premature failure[4,17–24]. Volume change, strength loss, and a reduction in the resilient modulus are a few of the physical and mechanical properties that can be induced by WDC in stabilized aggregate bases[1]. Zaman et al.[19] investigated the impact of WDC and FTC on resilient modulus values of cement-kiln-dust-stabilized Meridian limestone aggregate. Freezing/thawing proves more damaging than wetting/drying at low deviator stresses, with initial freeze/thaw stages causing significant strength reduction; wetting/drying induces greater strength reduction at high deviator stresses. The resilient modulus decreases as WDC and FTC increase, according to a study conducted by Diagne et al.[25] to assess the properties of base courses made from recycled materials. Khoury et al.[26,27] investigated the impact of moisture fluctuations subsequent to compaction on the unconfined compressive strength (UCS), modulus of elasticity (E), and resilient modulus (M_R) of cementitious stabilized subgrade soils. The stabilizers utilized in these soils were hydrated lime and Class C fly ash (CFA). Prior to evaluating M_R, UCS, and E, compacted specimens with varied stabilizer ratios (10% CFA and 6% lime) were either dried or wet. The findings demonstrated that drying increased M_R, UCS, and E, while soaking decreased these values.

Over the past few years, there has been rapid development in the field of artificial intelligence techniques. This development has led to the emergence of machine learning (ML) algorithms that have been proposed and are now widely used in various fields. ML applications have transformed the way how complex problems can be tackled using new and innovative solutions. Due to their learning ability, ML algorithms became a desirable tool for revealing relationships between many soil parameters. Therefore, the growing interest in studying the potential applications of ML algorithms on geotechnical issues has been witnessed in the past decades[28–38]. Furthermore, several researchers have also utilized ML algorithms to solve some other specific problems[39–42]. Researcher used ML algorithms to accurately calculates the resilient modulus (M_R) such as Khoury and Zaman[4] employed a least squares (LS) regression model to develop a correlation amongst the M_R and the following variables: the ratio of calcium oxide to SAF (silica, alumina, and ferric oxide compound), the maximum dry density to the optimum moisture content ratio, deviator stress, and confining stress.

Malouf et al.[43] used Support Vector Regression (SVR) approach for determining M_R under WDC in his study. Support Vector Regression (SVR) was used by Maalouf et al.[43] to find M_R under WDC in his work. The evaluation performed in this research exhibits the potential efficacy of the SVR approach in predicting the responses of M_R values induced by WDC. Comparative analyses performed between the SVR and LS methods underscore that the SVR outcomes significantly surpass the conventional LS technique. On the basis of a comparison of six data sets and the algorithms Kernel Ridge Regression (KRR), SVM, and Least Squares Support Vector Machines (LS-SVM), Maalouf and Homouz[44] determined that the TR-KRR algorithm is both as accurate as and significantly faster than the others. Ghanizadeh and Rahrovan[45] used ANN approach for the prediction of M_R under WDCs and compared them with SVM. Comparing the results of modeling resilient modulus using ANN with modeling using SVM confirms that ANN is more accurate than the SVM approach. Ghanizadeh et al.[46] used Adaptive Neuro-Fuzzy Inference System (ANFIS) for prediction of M_R under WDCs of aggregate bases. Results exhibited a high degree of model accuracy, with coefficients of determination (R^2) for the training and testing data sets are 0.9669 and 0.9625, respectively, and 0.9655 for the whole dataset. Kaloop et al.[1] developed three models in their study Particle Swarm Optimization Algorithm-Extreme Learning Machine (PSO-ELM), Particle Swarm Optimization-based Artificial Neural Network (PSO-ANN) and Kernel ELM (KELM) for the prediction of M_R and found that PSO-ELM has high accuracy than PSO-ANN and KELM. Ghanizadeh et al.[47] developed Gaussian Process Regression (GPR) for prediction of M_R and compared them with SVM and PSO-ELM. The results indicate that GPR has high accuracy with ($R^2 = 0.995$) than SVM and PSO-ELM. Khan et al.[15] evaluated the effect of WDC on the M_R of CaO-stabilized aggregate bases and cementitious materials, both of which are critical for pavement long-term service life. They created two models using ANN and Gene Expression Programming (GEP), which are ML approaches that can learn complex nonlinear correlations from data without requiring explicit assumptions or equations. The GEP beat the ANN in terms of accuracy, efficiency, and generalization ability while predicting the M_R of stabilized aggregate bases under WDC.

The extensive literature review demonstrates that computational techniques are quite capable of predicting the M_R. However, researchers and professionals predicted the M_R using a variety of computational models and datasets. The SHapley Additive exPlanations approach for describing the importance and participation of input variables that influence the resilient modulus of stabilized base material with various additives—Rhyolite, Richard Spur, Sawyer, and Meridian using cementitious materials, subjected to WDC has not been investigated. Furthermore, the LSTM model has not been implemented and compared. As a result, it is difficult to identify which computational approach is suitable for predicting the M_R. Still, it is noted that this field, is currently being investigated. Thus, the following problems are attempted to be addressed in this paper: (1) providing an accurate and efficient LSTM model for predicting the M_R of stabilized base material with various additives—Rhyolite, Richard Spur, Sawyer, and Meridian using cementitious materials, under WDC; (2) examining the prediction accuracy of the best LSTM model against that of existing ML models; (3) describing the significance and contribution of input variables that affect the M_R of stabilized base material with various additives under WDC using the SHAP method; and (4) development of online graphical user interface for simulating developed LSTM model for further application.

S. No.	WDC	CSAFR	DMR	σ_3	σ_d	M_R
1	0	0.130	2.34	138	69	1681
2	0	0.130	2.34	138	138	1784
3	0	0.130	2.34	138	208	2210
...	...	...	...	...	...	...
702	30	0.510	3.37	34.5	208	2043
703	30	0.510	3.37	34.5	277	2250
704	30	0.510	3.37	0	277	1632
Min	0	0.113	2.34	0	69	585
Max	30	0.51	4.63	138	277	9803
Mean	12.79545	0.254602	3.266051	70.12713	171.8182	3684.058
SD	11.1579	0.182769	0.711926	48.86403	77.63804	1860.495

Table 1. Input and output data for the current study.

Statistical Parameters	Dataset	WDC	CSAFR	DMR	σ_3	σ_d	M_R
Min	T	0.00	0.11	2.34	0.00	69.00	585.00
	T*	30.00	0.11	2.48	0.00	69.00	1373.00
Max	T	30.00	0.51	4.63	138.00	277.00	9803.00
	T*	30.00	0.51	4.40	138.00	277.00	7617.00
Mean	T	8.49	0.25	3.25	70.65	171.21	3836.16
	T*	30.00	0.28	3.33	68.02	174.23	3076.72
SD	T	7.93	0.18	0.72	48.96	77.59	1915.50
	T*	0.00	0.19	0.67	48.61	78.08	1479.12

Table 2. Training and testing dataset parameter statistics. Note: T: Training; T*: Testing.

Dataset

In this research, the experimental data were collected from Maloof et al. study[43], In this study, four aggregates—Rhyolite, Richard Spur, Sawyer, and Meridian—were stabilized utilizing cementitious materials, subjected to WDC, and assessed for M_R. Meridian is a limestone aggregate that comprises around 97% calcium carbonate ($CaCO_3$). Richard Spur, and limestone aggregate, has a less $CaCO_3$ proportion than Meridian, at 87% approximately. Sawyer aggregate, a sandstone aggregate, contains approximately 94% SiO_2. Hanson is an aggregate variety of rhyolite. Samples were prepared with optimum moisture content and maximum dry density, then cured for 28 days in a wet environment maintaining a temperature of 21℃ (70℉) and a regulated relative humidity of 90% (2.5%). Specimens underwent 0, 8, 16, and 30 WDC, with zero being reference control specimens that received no WDC. For more details on material properties, specimen preparation, and the WDC procedure, the reader might refer to Maalouf et al.[43] research. The parameters σ_d and σ_3 have a major impact on material behavior, clarify relationships, and provide insights into mechanical responses. This strategy improves feature engineering and model performance. The resilient modulus outcomes are composed of 704 records (see Appendix A, Tables A1 and A2) and five features, where WDC, calcium oxide to silica, alumina, and ferric oxide compound ratio (CSAFR), Maximum dry density to the optimal moisture content ratio (DMR), deviator stress (σ_d), and confining stress (σ_3) are regarded input parameters, while M_R is taken as an output parameter. Table 1 shows the experimental results for M_R testing, mentioning the minimum (Min), maximum (Max), mean, and standard deviation (SD) of the input and output variables. The database, as shown in the table, includes input parameters i.e., WDC, CSAFR, DMR, σ_d, and σ_3, and one output parameter i.e., resilient modulus (M_R).

To determine which representation was the most resilient, a statistical analysis was performed on the input and output variables of the training and testing datasets (refer to Table 2). The minimum and maximum values indicate the data spread out, mean shows the central value for the dataset and standard deviation indicates how much variation exists from the mean for training and testing datasets respectively. The acquired data is divided into training (80%) and testing (20%) datasets. It was attained through trial and error. Previous studies show that the M_R of stabilized base material with various additives is a function of WDC, CSAFR, DMR, σ_d, and σ_3[21,43,48].

All of the input and output variables under study were correlated using the Pearson correlation coefficient (r). Each cell in the plot has a correlation coefficient, which represents the strength of relationship between two factors. Figure 1 depicts the correlations between several parameters in the dataset. The "r" between the various parameters in Fig. 1 is evaluated as follows:

$$r(m, m') = \frac{\mathrm{cov}(m, m')}{\sigma_m \sigma_{m'}} \tag{1}$$

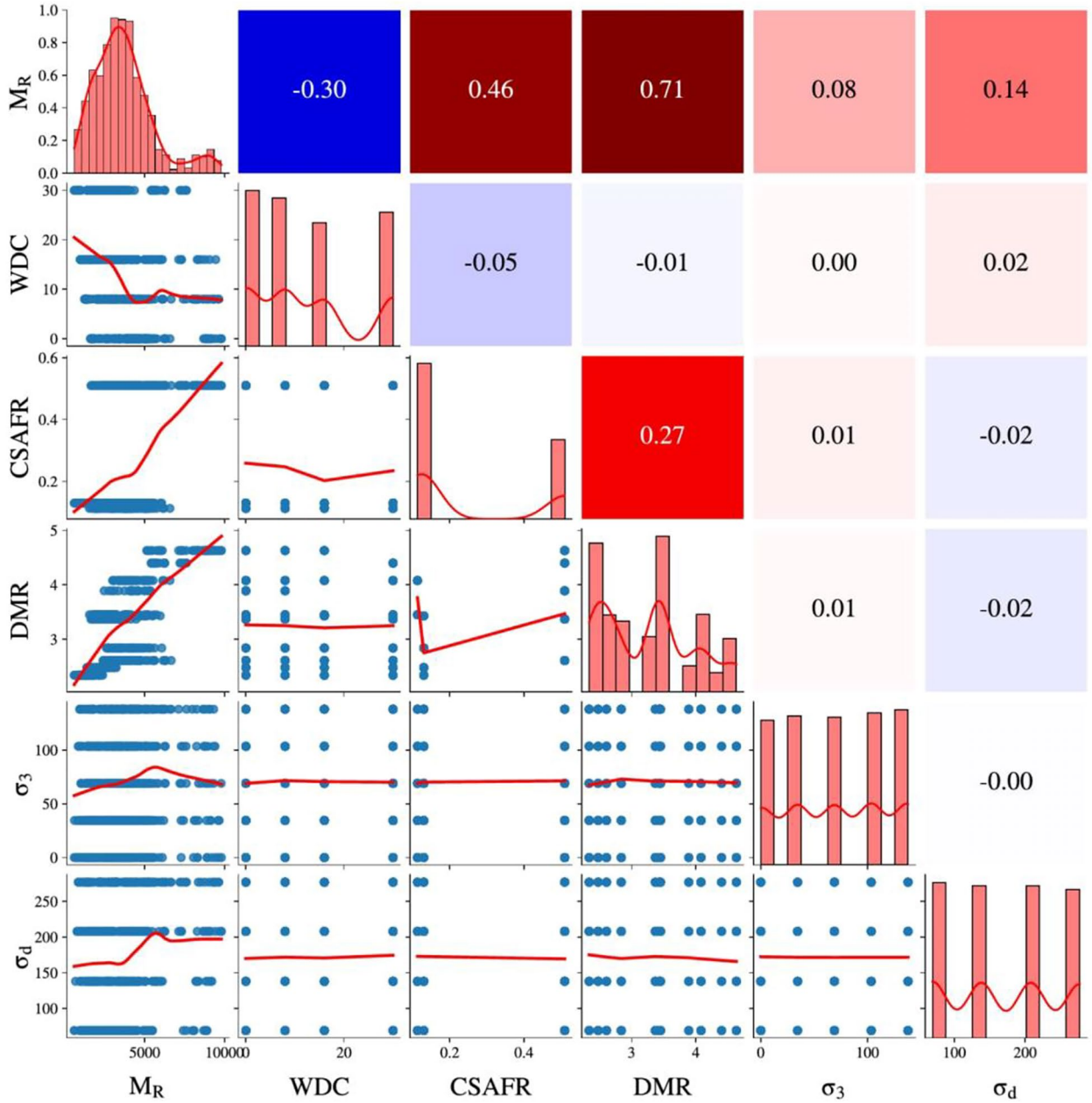

Fig. 1. Correlation among different parameters in the dataset.

where cov = covariance, σ_m = the standard deviation of m while $\sigma_{m'}$ = the standard deviation of m'. The coefficients range from − 1 to 1, indicating the strength and direction of the correlation. One notable observation is the strong positive correlation between M_R and DMR. As DMR increases, M_R tends to increase as well. Additionally, there's a moderate positive correlation between M_R and the CSAFR, suggesting a potential link between these two factors. Interestingly, WDC exhibit a weak negative correlation with M_R, implying that higher WDC values might be associated with slightly lower resilient modulus values. Conversely, the correlation between WDC and other parameters is generally minimal, as most correlation coefficients are close to zero. DMR displays a strong positive correlation with M_R, indicating that these two parameters tend to increase in tandem. Moreover, a weak positive correlation between DMR and CSAFR suggests some degree of alignment between these factors. The σ_3 and σ_d show weak correlations with other parameters, as most correlation coefficients are near zero.

LSTM modeling

LSTM networks are a type of recurrent neural network (RNN) architecture capable of detecting long-term dependencies and patterns in sequential data. They were created to overcome the vanishing gradient issue that

afflicted traditional RNNs, restricting their capacity to accurately capture long-term relationships in sequences. The LSTM has been utilized in various sectors for data prediction and proven excellent performance on a wide range of problems[49–53]. Hochreiter and Schmidhuber[54,55] designed LSTM to address the problem posed by classical RNNs[56] and ML methods. The central component of an LSTM model is a memory cell known as a 'cell state' that maintains its state across time. The horizontal line across the top of Fig. 2 represents the cell state. It can be likened to a conveyor belt through which information flows unaltered. The LSTM is implemented in Python with the Keras library.

A typical LSTM unit consists of a cell, an input gate, an output gate, and a forget gate. The cell holds values for arbitrary time intervals, and the three gates regulate the flow of information into and out of the cell. Forget gates determine what information to discard from a previous state based on a comparison of the previous state and the current input, resulting in a value between 0 and 1. A number of one suggests that information should be maintained, whereas a value of zero indicates that information should be deleted. Input gates, like forget gates, determine which new information to store in the current state. Output gates control the information that is output from the current state by assigning a value between 0 and 1, while taking past and current states into account. This selective output of important information enables LSTM networks to sustain resilient long-term dependencies, allowing for accurate predictions across multiple time steps. Equations (2)–(7) depict the processes that occur in an LSTM cell.

$$f_t = \sigma_g(W_f x_t + U_f h_{t-1} + b_f) \tag{2}$$

$$i_t = \sigma_g(W_i x_t + U_i h_{t-1} + b_i) \tag{3}$$

$$o_t = \sigma_g(W_o x_t + U_o h_{t-1} + b_o) \tag{4}$$

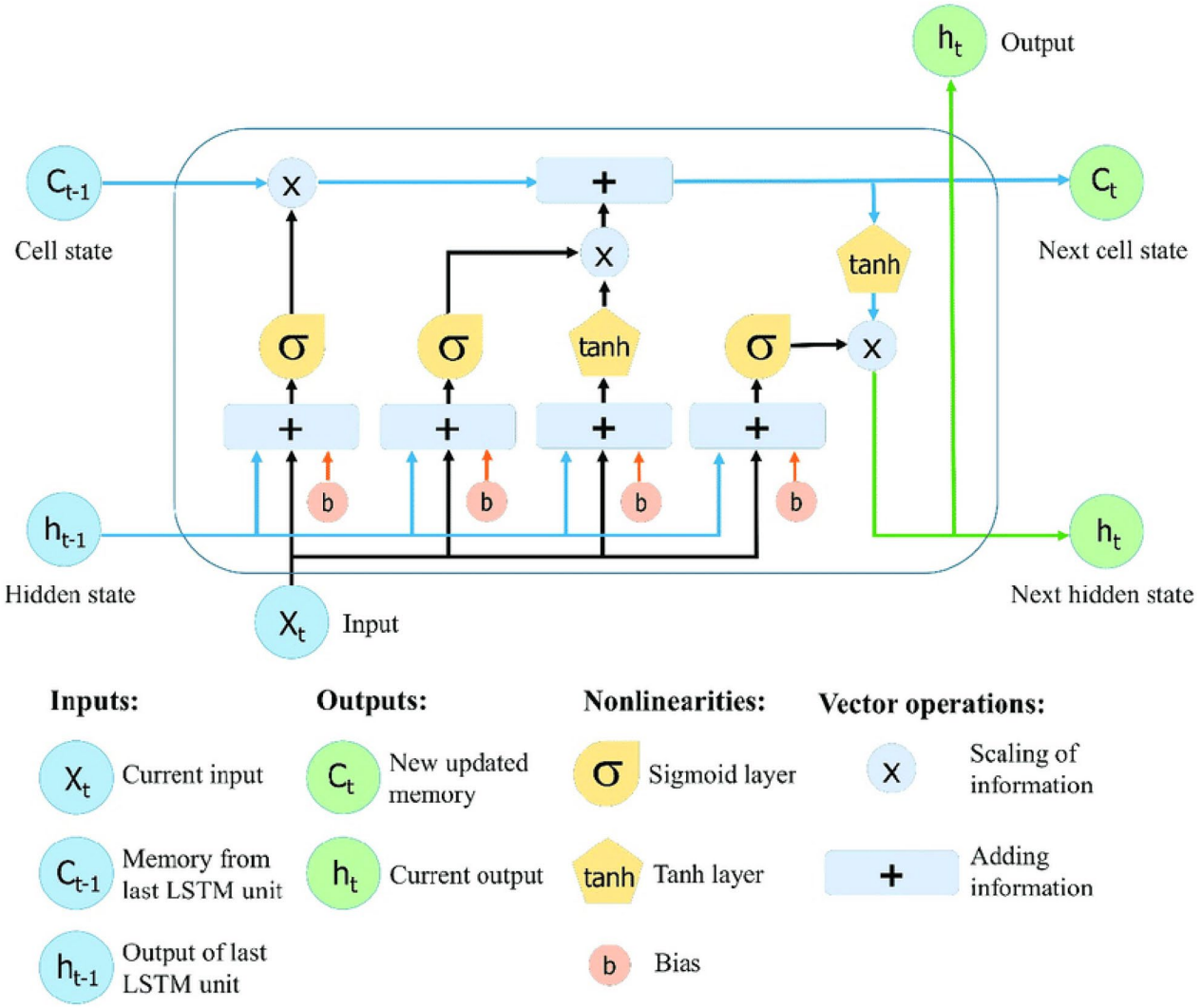

Fig. 2. Architecture of LSTM Model.

$$c'_t = \sigma_g(W_c x_t + U_c h_{t-1} + b_c) \quad (5)$$

$$c_t = f_t \odot c_{t-1} + i_t \odot c_{t-1} \quad (6)$$

$$h_t = o_t \odot \sigma_h(c_t) \quad (7)$$

Where f_t is the forget gate, i_t is the input gate, o_t is the output gate, σ is the sigmoid activation function, h_t is the hidden state, c_t and c'_t is the cell state, ⊙ represents element-wise multiplication, b_f, b_i, b_o, and b_c are bias vectors. W_f, W_i, and W_i weight for the forget gate, input gate and output gate respectively.

Proposed LSTM Model

The process involves acquiring a dataset (see Appendix A, Tables A1 and A2), dividing it into training (80%) and testing (20%) datasets, and then constructing an LSTM model within a chosen framework. This LSTM model is trained using the training data through multiple epochs, where the model's parameters are optimized using an optimization algorithm to minimize a selected loss function. Following training, the model's performance is assessed on the testing set as shown in Fig. 3.

The deep learning techniques employed in this study were put into action using the Python programming language within a Python idle environment. The execution of these models took place on a Windows 10 system equipped with an Intel(R) Core i3–5th Generation central processing unit and 4 GB of random access memory. the process commences by loading the dataset and segregating the characteristics and the target variable. Following this, the characteristics are standardized utilizing the StandardScaler technique from the 'sklearn. preprocessing' module to standardize the input features before feeding them into the model. StandardScaler is a common technique used in machine learning to normalize the input data so that it has a mean of 0 and a standard deviation of 1. The LSTM model's structure is defined, encompassing LSTM layers, dropout for regularization, and dense layers. This model is compiled employing an optimizer and a loss function. Subsequently, the model is trained on the training dataset and used to predict output variable on the test dataset. The hyperparameters chosen for the LSTM-based model are crucial in determining its effectiveness in analyzing sequential data. The model comprises two LSTM layers, each containing 50 hidden units. The use of the rectified linear unit (relu) activation function within the LSTM layers increases nonlinearity, which improves the ability of the model to capture complicated patterns in the data. To mitigate overfitting, a dropout rate of 0.2 is employed, which randomly deactivates a portion of neurons during training, thus aiding in generalization. The architecture also incorporates two dense layers: the first consists of 10 units, followed by a single output unit. By employing relu activation in the initial dense layer and linear activation in the final one, the model gains the capacity to decipher intricate data relationships while producing continuous outputs. The rmsprop optimizer is applied to facilitate efficient parameter optimization by adaptively adjusting learning rates. The choice of the mean absolute error (MAE) as the loss function assesses prediction accuracy by quantifying the magnitude of errors. The model undergoes training for 500 epochs, each involving a batch size of 4, striking a balance between computational efficiency and convergence precision (see Table 3). These hyperparameters collectively shape the model's architecture, poised to extract meaningful insights from sequential data with precision and efficiency.

Evaluation parameters of LSTM model

Several regression performance indices like R-squared (R^2), Root Mean Squared Error (RMSE), Mean Absolute Error (MAE), Mean Squared Error (MSE), Mean Absolute Percentage Error (MAPE), and Mean Absolute

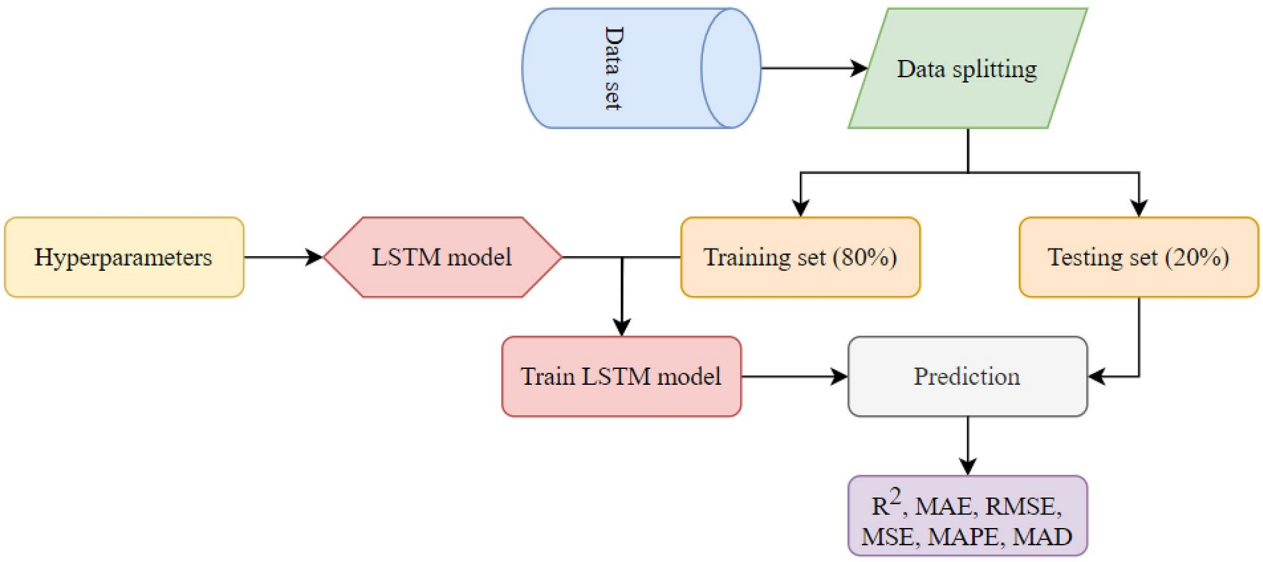

Fig. 3. Workflow of proposed LSTM Model.

Hyper-parameter	Value
Number of LSTM layers	4
Number of hidden units per LSTM layer	300
Activation function for LSTM layers	relu
Dropout rate for LSTM layers	0.1
Number of dense layers	2
Number of units per dense layer	300 and 1
Activation function for dense layers	relu and linear
Optimizer	rmsprop
Loss function	mean_absolute_error
Number of epochs	500
Batch size	4

Table 3. Hyper-parameters used for LSTM Model.

	Inputs					Training		Testing	
Model	WDC	CSAFR	DMR	σ_3	σ_d	R^2	RMSE	R^2	RMSE
A	√	√	√	√	√	0.995	128.315	0.980	242.463
B	√	√	√	√		0.920	533.233	0.902	566.948
C	√	√	√		√	0.949	423.977	0.939	445.568
D	√	√	√			0.905	583.745	0.903	540.15

Table 4. Results for testing dataset and training dataset.

Deviation (MAD) are calculated during the evaluation stage. These metrics serve to gauge the efficacy of the model's performance, shedding light on the extent to which the model's predictions correlate with the actual target values. The formulations used to calculate these performance metrics are expressed in Eqs. (8)–(13)[57–66].

$$\mathrm{R}^2 = \frac{\sum_{i=1}^{n}(d_i - d_{mean})^2 - \sum_{i=1}^{n}(d_i - y_i)^2}{\sum_{i=1}^{n}(d_i - d_{mean})^2} \tag{8}$$

$$RMSE = \sqrt{\frac{1}{N}\sum_{i=1}^{n}(d_i - y_i)^2} \tag{9}$$

$$MAE = \frac{1}{N}\sum_{i=1}^{n}|(y_i - d_i)| \tag{10}$$

$$MAPE = \frac{1}{N}\sum_{i=1}^{n}\left|\frac{d_i - y_i}{d_i}\right| * 100 \tag{11}$$

$$MSE = \frac{1}{N}\sum_{i=1}^{n}(y_i - d_i)^2 \tag{12}$$

$$MAD = \frac{1}{N}\sum_{i=1}^{n}|(y_i - d_{mean})| \tag{13}$$

where d_i is the ith observed value, y_i is the ith predicted value, d_{mean} is the mean value of the observed values, n is the training or testing samples and N indicates the total number of samples.

Results and discussion

LSTM models comparative performance

The LSTM was the data analysis model of choice for this work. The LSTM accuracy is determined by the number of hidden layers, the number of units in each layer, the activation function, the dropout rate, the optimizer, and the loss function. The settings of these parameters that provide the best generalization are often chosen from a range of different values (normally user defined). Table 4 shows the values of the parameters chosen for this study. In this analysis four different LSTM models are developed with different combinations of input variables. Model A considers all five input variables, model B considers four input variables by excluding σ_d, model C considers four input variables by excluding σ_3, and model D considers three input variables by excluding both σ_d and σ_3. The performance of these four LSTM models is demonstrated in Figs. 4, 5, 6 and 7, where the predicted values of M_R are compared with actual values of M_R for both training and testing subsets.

The Model A plots (see Fig. 4) depict the model's performance on both the training and testing datasets. It is evident that the model fits well for both sets, as a large number of data points are in close proximity to the

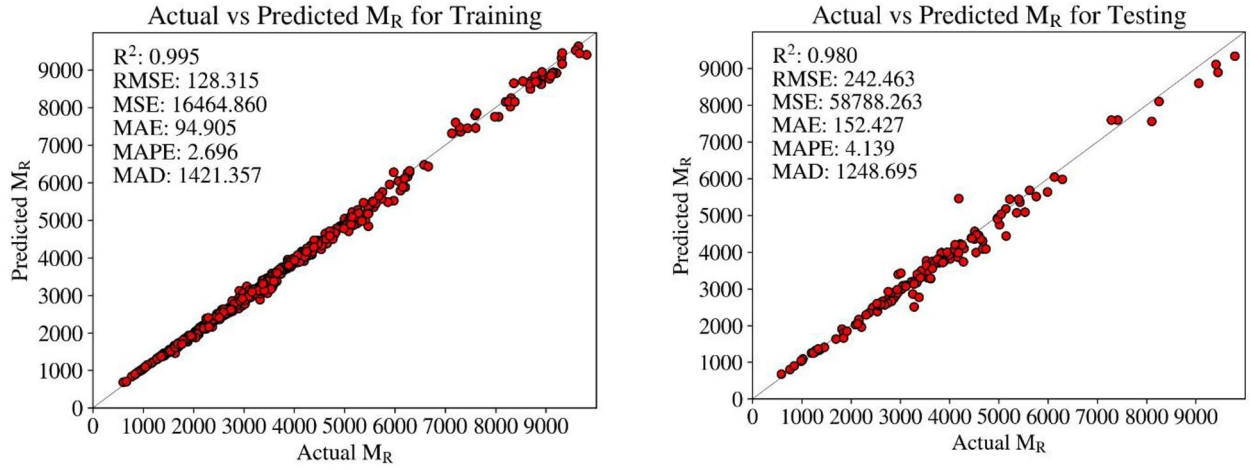

Fig. 4. The predicted versus measured resilient moduli for model "A" based on the training and testing datasets.

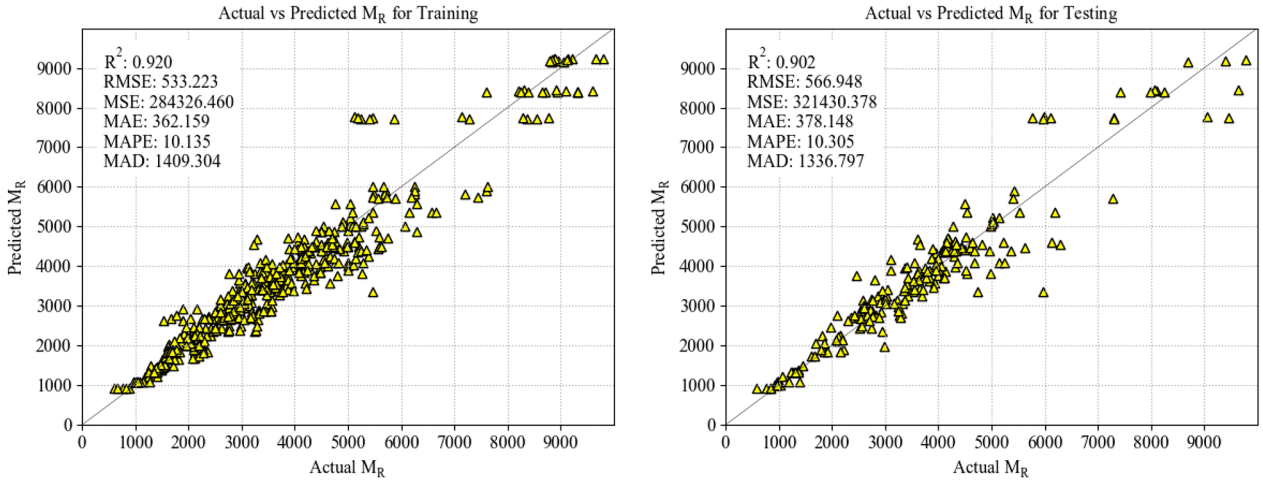

Fig. 5. The predicted versus measured resilient moduli for model "B" based on the training and testing datasets.

line with $R^2 = 0.995$ and 0.980 in training and testing datasets respectively. The values of RMSE (128.315), MSE (16464.860), MAE (94.905), MAPE (2.696), and MAD (1421.357) for training dataset and RMSE (242.463), MSE (58788.263), MAE (152.427), MAPE (4.139), and MAD (1248.695) for testing dataset indicating that the model A has a low error rate when compared to the models B, C and D. Furthermore, The ANN model yielded the values for MAE of 245, respectively, the GEP model manifested 764 respectively[15], whereas the GPR model resulted R^2 (0.9979), RMSE (85.5743), MAPE (1.2873), MAD (1060.7312), and MAE (47.4161) in training dataset and R^2 (0.9849), RMSE (242.6246), MAPE (4.3140), MAD (1068.1651), and MAE (159.0427) in testing dataset with five inputs of Model A[47]. The GPR and LSTM models almost showed compatible performance based on their performance indices but exceeded in accuracy in comparison with the GEP and ANN models.

The Model B plots (see Fig. 5) show the actual vs. predicted M_R values for training and testing sets, after removing σ_d variable from input. Comparing these plots to the previous ones, where five input variables were utilized, it is clear that excluding variable σ_d has a detrimental impact on the model's performance. The accuracy of predictions is reduced, and the errors are increased when σ_d is removed from the model. This finding suggests that σ_d is an essential and relevant variable that significantly influences M_R concentration. By eliminating this variable, the model loses valuable information critical for making accurate predictions. Therefore, it is evident that σ_d plays a crucial role in the model's ability to capture the complexities and variations in M_R concentration.

The Model C plots (see Fig. 6) show the actual vs. predicted M_R values for both viz. training and testing sets, after removing σ_3 variable from input. The Model C plots clearly demonstrate that σ_3 does not play a significant role in determining M_R.

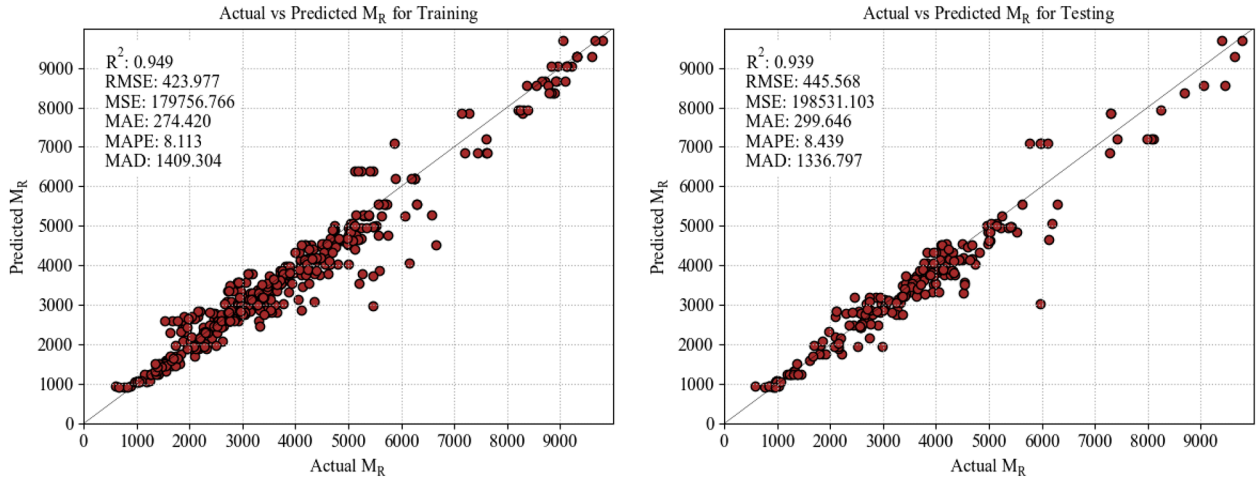

Fig. 6. The predicted versus measured resilient moduli for model "C" based on the training and testing datasets.

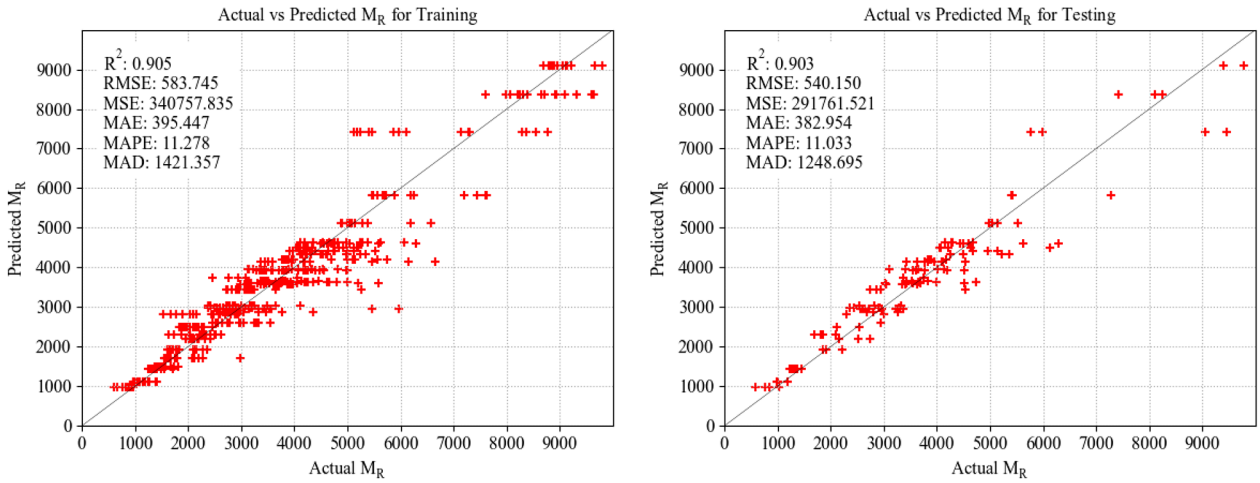

Fig. 7. The predicted versus measured resilient moduli for model "D" based on the training and testing datasets.

The Model D plots (see Fig. 7) show the actual vs. predicted M_R values for both the training and testing datasets, after removing the σ_3 and σ_d variables from the input set. Comparing these plots to the previous ones, where four input variables were utilized, it becomes apparent that removing variable σ_d has a negative impact on the model's performance. Although the reduction in accuracy and increase in error are slight, they are still noticeable. This observation suggests that σ_d is an important and relevant variable that significantly influences M_R concentration. By removing σ_3 and σ_d variables from the model, valuable information related to M_R concentration is lost, which affects the model's ability to make accurate predictions.

The accuracy of all developed models at predicting M_R values is depicted in Fig. 8a-d for the training dataset and Fig. 9a-d for the testing dataset. The LSTM Model A (see Fig. 8 (a) and Fig. 9 (a)) provided the most reliable prediction, as seen in these graphs. Except for a few noise points, this is demonstrated by the increased aggregation of data around the y axis (i.e., $y=0$). In contrast to the other models, namely Models B, C, and D, the comparison results are sufficiently consistent, indicating that the proposed LSTM Model A is capable of predicting M_R values.

Comparison with literature

Table 5 lists the performance indices' values as well as the various input parameter combinations. The results shown in Table 5 demonstrate that LSTM model A works better when all the input factors are used with R^2 of 0.995 and MSE of 16464.860. This accuracy is significantly more than the R^2 value of 0.6851 for the LS approach[43] and R^2 value of 0.9593 for SVM method[43] as Table 5 indicates, on any combination. In addition, with

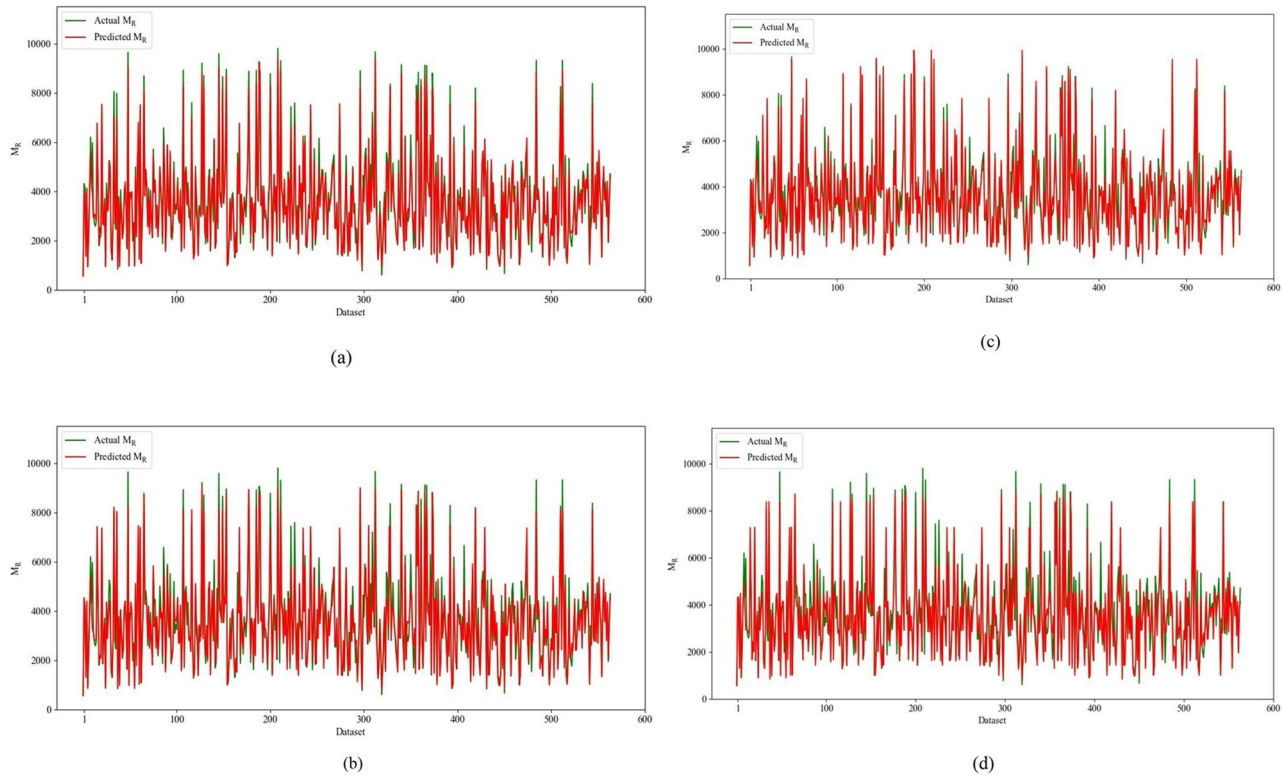

Fig. 8. Comparison of the LSTM Models results in the training dataset (**a**) Model A, (**b**) Model B, (**c**) Model C, and Model D in predicting M_R values.

the exception of model A, LSTM models B and D outperformed the LS and SVM approaches, with R^2 values of 0.920 and 0.905, respectively. As can be seen, depending on the number of input parameters, the accuracy of the LSTM model can be more than the SVM and LS methods except in model C. However, if all input parameters are considered, the accuracy of the LSTM model is much higher than the SVM and LS models, so that the R^2 for the LSTM model is 0.995 more than the R^2 (0.6400) for the SVM model and R^2 (0.6851) for the LS model. Furthermore, the scatter plots (Figs. 4 and 5, and 7) show that the LSTM model outperforms the LS and SVM approaches in predicting M_R, with variations around the 45° line. In general, the LSTM model A outperforms in terms of generalization and reliability, yielding superior prediction outcomes.

SHAP Analysis

The SHAP method effectively depicts the impact of each input variable on an ML model's predictions. The idea is based on cooperative game theory, in which the Shapley values are employed to evaluate each player's contribution to the coalition. Equation (14) determines the Shapley values Φ_i, which are the core of this methodology. F is the set of all input features, and S is a subset of F that excludes the feature with index i. Equation (14) defines the impact of a feature as the differences in model outputs when a feature is included and deleted from the collection of input features.

$$\Phi_i = \sum_{S \subseteq F\{i\}} \frac{|S|!\,(|F| - |S| - 1)!}{|F|!} [f_{S\cup\{i\}}(x_{S\cup\{i\}}) - f_S(x_S)] \tag{14}$$

Figure 10 shows a SHAP summary graphic that ranks each input feature based on its influence on the output of the LSTM model A. Each feature's SHAP value indicates its contribution to the model's prediction. Positive SHAP values suggest that the feature increases the prediction, while negative values indicate a decrease (see Fig. 10). Figure 10 shows that DMR is the most important factor in predicting M_R, followed by the WDC. It can be seen that increasing the DMR and WDC, has an increasing effect on model predictions. The same is validated from the literature that DMR is the most influential input followed by WDC in the GEP model[15].

The SHAP values of all features added together indicate why the prediction differed from the baseline. This enables us to decompose a prediction in the graph depicted in Fig. 11. The predicted model output value is 4325.87, whereas the base value is 3733. The greater the size of the arrow, the greater the impact. A red arrow moves the result to the right (increases the model output value), while a blue arrow moves the result to the left (decreases the model output value). The greatest influence comes from σ_3 being 1.39. Despite the fact that the DMR value has a significant effect on the prediction.

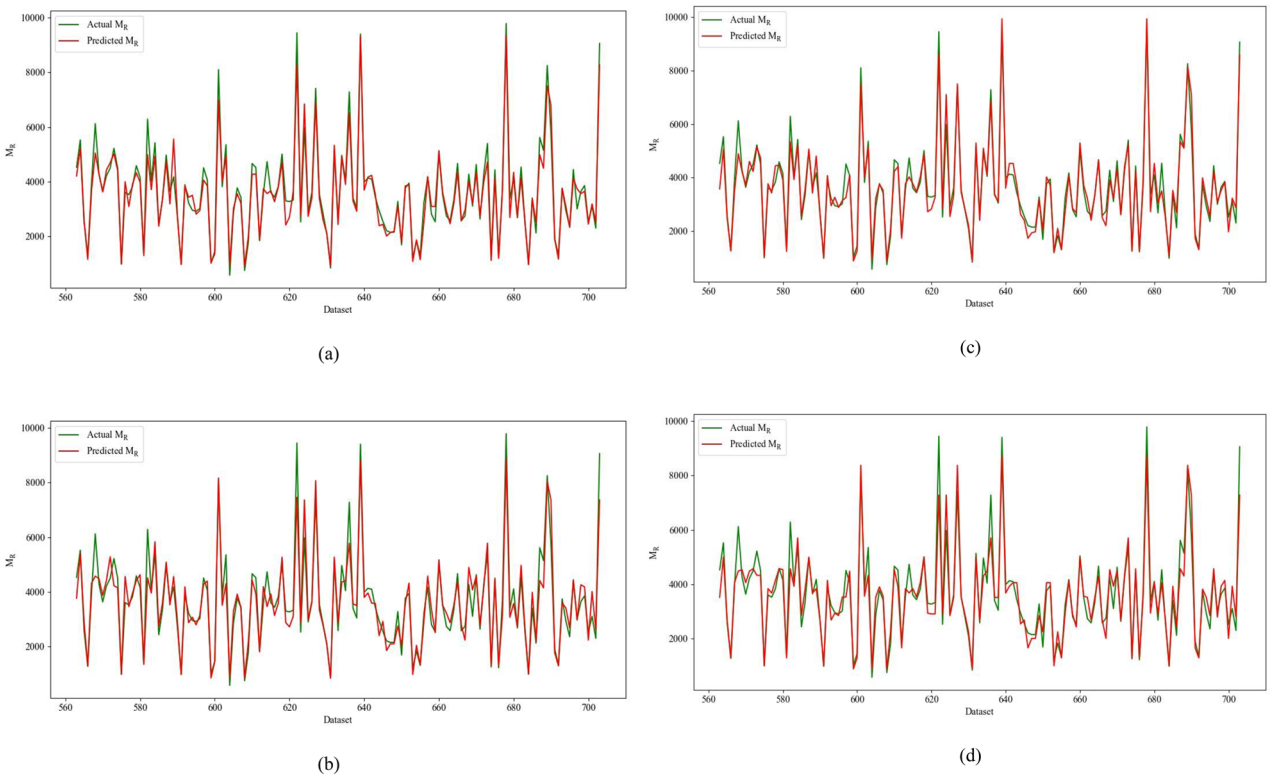

Fig. 9. Comparison of the LSTM Models results in the testing dataset (**a**) Model A, (**b**) Model B, (**c**) Model C, and Model D in predicting M_R values.

	Inputs					SVM [43]		LS [43]		LSTM (This study)	
Model	WDC	CSAFR	DMR	σ_3	σ_d	R^2	MSE	R^2	MSE	R^2	MSE
A	√	√	√	√	√	0.6400	1,287,300	0.6851	1,079,400	0.995	16464.860
B	√	√	√	√		0.8750	435,270	0.6581	1,172,200	0.920	2844326.460
C	√	√	√		√	0.9593	137,870	0.6805	1,094,800	0.949	179756.766
D	√	√	√			0.9001	352,290	0.6538	1,186,600	0.905	340757.835

Table 5. Comparative performance of LSTM models with models developed in literature.

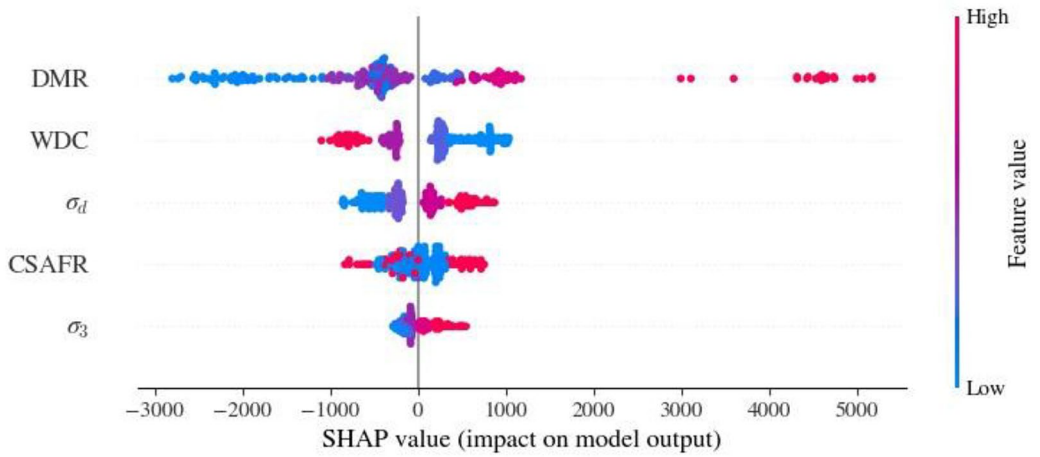

Fig. 10. SHAP summary plot for the LSTM model A.

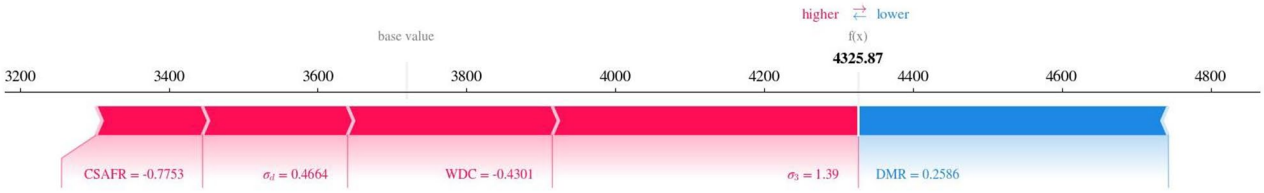

Fig. 11. SHAP force plot for the LSTM model A.

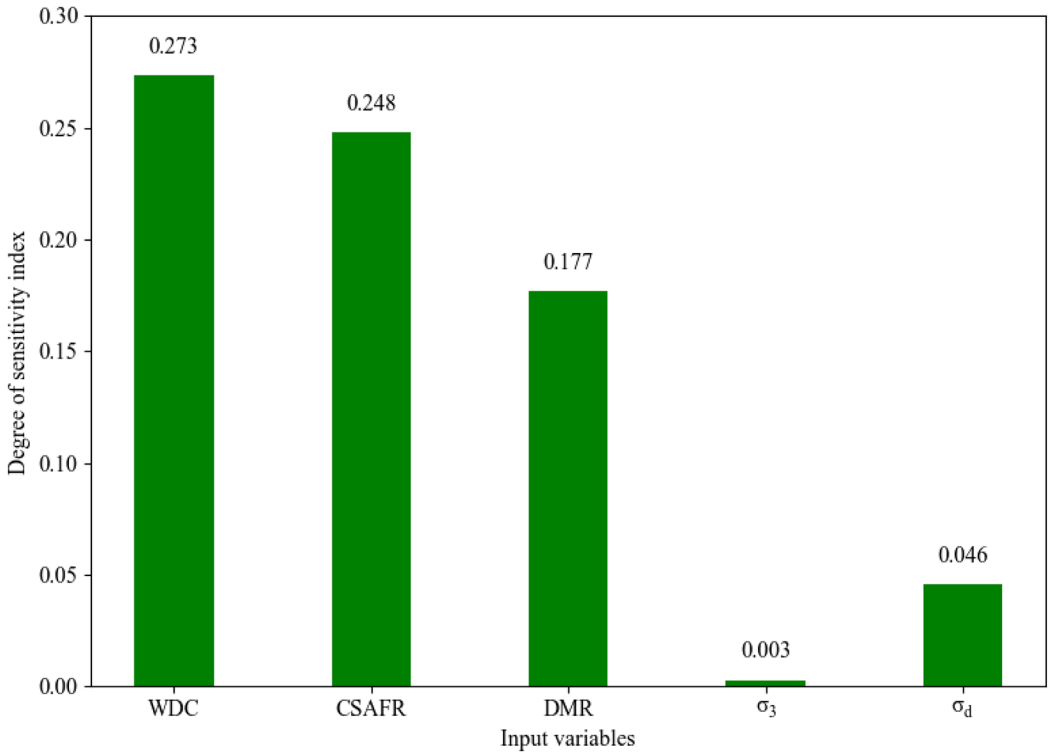

Fig. 12. Degree of sensitivity analysis for predicted M_R.

Sensitivity analysis

Sensitivity analysis is a technique that helps to understand how different factors or inputs affect the output of a model. The Cosine amplitude approach is used to calculate the relationship between the M_R and the input parameters. The following equation is used to calculate the degree of sensitivity index for each input parameter.

$$R_{ij} = \frac{\sum_{j=1}^{n} x_{ij} y_j}{\sqrt{\sum_{j=1}^{n} x_{ij}^2 \sum_{j=1}^{n} y_j^2}} \tag{15}$$

where R_{ij} shows the degree of sensitivity index of each input parameter, x_{ij} presents the i^{th} independent variable for the j^{th} dependent variable and y_j represents the dependent variable for the j^{th} data point. Strong correlation between the input and output variable is indicated by a R_{ij} value close to 1, whereas weak correlation between the input and output variable is indicated by a R_{ij} value close to 0. WDC has the highest degree of sensitivity index (0.273), as seen in Fig. 12, which means that changing WDC has the most impact on M_R. On the other hand, σ_3 has the lowest degree of sensitivity index (0.003), which means that changing σ_3 has the least impact on M_R. The degree of importance can be presented as WDC > CSAFR > DMR > σ_d > σ_3.

Graphical user interface

Graphical User Interface (GUI) is user-friendly tool that leverage ML-based prediction model to predict the M_R. The package has a broad collection of LSTM algorithm. The prediction model does not need to be retrained for M_R estimation because it was already trained on experimental data points. The GUI is well-designed and simple to use (see Fig. 13). Once the user enters the required parameters into the GUI, the trained ML algorithm

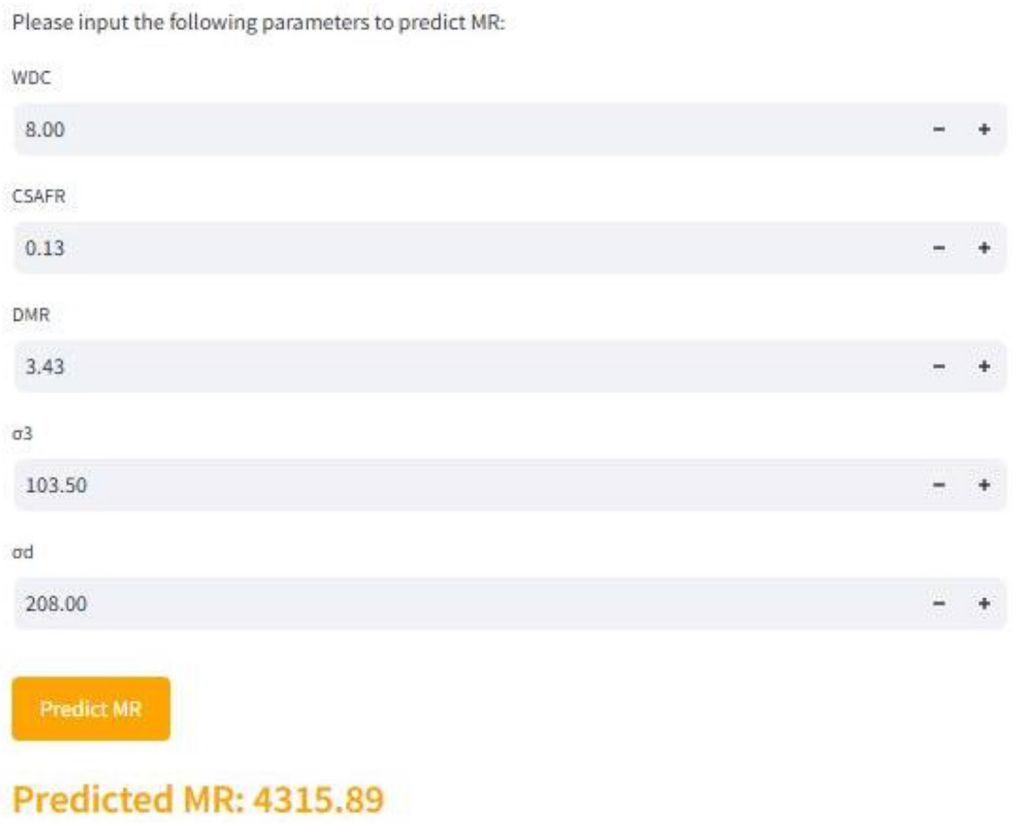

Fig. 13. The developed GUI.

can accurately predict the M_R. When compared to other approaches, the GUI offers fast and cost-effective M_R estimation with great accuracy. Furthermore, it is a significant platform for academics interested in accumulating M_R-related datasets. The computing time for an LSTM model is less than 60 s. The GUI is available online at https://lstmmrprediction-7m6j96pn2qmxemkeqxuzaq.streamlit.app/.

Conclusions

LSTM model is developed in this study for the prediction of resilient modulus of stabilized base material with input parameters, including WDC, CSAFR, DMR, σ_d, and σ_3. The main findings are given as:

(1) Pearson correlation coefficient results indicate the strength of the association between two variables: DMR and CSAFR have a strong positive correlation with M_R, while WDC has a negative correlation with M_R. Furthermore, σ_3 and σ_d show a weak positive coorealtion with M_R in experimental data.

(2) Model "A" performs best with R^2 and RMSE values of 0.995 and 128.315 for the training set and 0.980 and 242.463 for the testing set, while model "D" performs lower with R^2 and RMSE values of 0.905 and 583.745 for the training set and 0.903 and 540.150 for the testing set. The results conclude that LSTM model A accuracy is significantly more than the R^2 value of 0.6851 for the LS approach and R^2 value of 0.9593 for SVM method reported in literature.

(3) The results showed that omitting the σ_d variable in model "B" resulted in a more substantial loss in model accuracy compared to excluding the σ_3 variable in model "C". This shows that the M_R of stabilized base materials is more influenced by deviator stress (σ_d) than by confining stress (σ_3), as evidenced by the greater impact on accuracy when σ_3 is omitted from the model. The DMR has the greatest influence in predicting the M_R, followed by the WDC and σ_d.

(4) The DMR was the most significant input variable according to the SHAP approach, followed by the WDC, σ_d, CSAFR, and σ_3.

(5) The sensitivity analysis unveiled that WDC held the highest level of significance in its contribution to M_R. Moreover, CSAFR and DMR were identified as the subsequent key factors. In contrast, σ_d and σ_3 demonstrated the least significance in the prediction of M_R values. The degree of importance can be presented as WDC > CSAFR > DMR > σ_d > σ_3.

(6) To enhance the prediction of the M_R for engineering challenges, a cutting-edge GUI for the LSTM-based model was meticulously developed.

In the future, a larger database can be established to further illustrate the adequacy of LSTM algorithm for the prediction of resilient modulus. The influences of other indicators on the prediction results are essential to be analyzed. The methodology can also be applied in other fields, such as the liquefaction-induced lateral spread, unconfined compressive strength of rocks, and settlement of shallow foundation.

Data availability

Data is provided within the manuscript or supplementary information files.

Appendix A

WDC	CSAFR	DMR	σ_3	σ_d	M_R
0	0.130	2.34	138	69	1681
0	0.130	2.34	138	138	1784
0	0.130	2.34	138	208	2210
0	0.130	2.34	138	277	2277
0	0.130	2.34	103.5	69	1652
0	0.130	2.34	103.5	138	1718
0	0.130	2.34	103.5	208	1914
0	0.130	2.34	103.5	277	2152
0	0.130	2.34	69	69	1619
0	0.130	2.34	69	138	1692
0	0.130	2.34	69	208	1849
0	0.130	2.34	69	277	2119
0	0.130	2.34	34.5	69	1609
0	0.130	2.34	34.5	138	1688
0	0.130	2.34	34.5	208	1835
0	0.130	2.34	34.5	277	2368
0	0.130	2.34	0	69	1612
0	0.130	2.34	0	138	1673
0	0.130	2.34	0	208	1796
0	0.130	2.34	0	277	2093
0	0.130	3.43	138	69	4387
0	0.130	3.43	138	138	4636
0	0.130	3.43	138	208	4995
0	0.130	3.43	138	277	5516
0	0.130	3.43	103.5	69	4318
0	0.130	3.43	103.5	138	4401
0	0.130	3.43	103.5	208	4755
0	0.130	3.43	103.5	277	5121
0	0.130	3.43	69	69	4290
0	0.130	3.43	69	138	4332
0	0.130	3.43	69	208	4671
0	0.130	3.43	69	277	4969
0	0.130	3.43	34.5	69	3907
0	0.130	3.43	34.5	138	4084
0	0.130	3.43	34.5	208	4104
0	0.130	3.43	34.5	277	4736
0	0.130	3.43	0	69	3968
0	0.130	3.43	0	138	4191
0	0.130	3.43	0	208	4198
0	0.130	3.43	0	277	5148
0	0.130	2.84	138	69	3218
0	0.130	2.84	138	138	3646
0	0.130	2.84	138	208	4334
0	0.130	2.84	138	277	4820
0	0.130	2.84	103.5	69	3112
0	0.130	2.84	103.5	138	3447
0	0.130	2.84	103.5	208	3943
0	0.130	2.84	103.5	277	4546
0	0.130	2.84	69	69	3123
0	0.130	2.84	69	138	3408
0	0.130	2.84	69	208	3949
0	0.130	2.84	69	277	4306

WDC	CSAFR	DMR	σ_3	σ_d	M_R
0	0.130	2.84	34.5	69	3141
0	0.130	2.84	34.5	138	3338
0	0.130	2.84	34.5	208	4012
0	0.130	2.84	34.5	277	4134
0	0.130	2.84	0	69	3113
0	0.130	2.84	0	138	3377
0	0.130	2.84	0	208	3888
0	0.130	2.84	0	277	4063
0	0.130	2.48	138	69	2585
0	0.130	2.48	138	138	2767
0	0.130	2.48	138	208	2843
0	0.130	2.48	138	277	3221
0	0.130	2.48	103.5	69	2601
0	0.130	2.48	103.5	138	2603
0	0.130	2.48	103.5	208	2707
0	0.130	2.48	103.5	277	3140
0	0.130	2.48	69	69	2559
0	0.130	2.48	69	138	2578
0	0.130	2.48	69	208	2640
0	0.130	2.48	69	277	2972
0	0.130	2.48	34.5	69	2586
0	0.130	2.48	34.5	138	2596
0	0.130	2.48	34.5	208	2754
0	0.130	2.48	34.5	277	3035
0	0.130	2.48	0	69	2557
0	0.130	2.48	0	138	2597
0	0.130	2.48	0	208	2718
0	0.130	2.48	0	277	2996
0	0.113	4.08	138	69	5081
0	0.113	4.08	138	138	5529
0	0.113	4.08	138	208	6199
0	0.113	4.08	138	277	6579
0	0.113	4.08	103.5	69	5013
0	0.113	4.08	103.5	138	5049
0	0.113	4.08	103.5	208	5140
0	0.113	4.08	103.5	277	5377
0	0.113	4.08	69	69	4893
0	0.113	4.08	69	138	5029
0	0.113	4.08	69	208	5046
0	0.113	4.08	69	277	5274
0	0.113	4.08	34.5	69	4994
0	0.113	4.08	34.5	138	5023
0	0.113	4.08	34.5	208	5050
0	0.113	4.08	34.5	277	5286
0	0.113	4.08	0	69	4889
0	0.113	4.08	0	138	4974
0	0.113	4.08	0	208	5085
0	0.113	4.08	0	277	5147
0	0.113	3.45	138	69	3872
0	0.113	3.45	138	138	4177
0	0.113	3.45	138	208	4701
0	0.113	3.45	138	277	5751
0	0.113	3.45	103.5	69	3884
0	0.113	3.45	103.5	138	3898
0	0.113	3.45	103.5	208	4001
0	0.113	3.45	103.5	277	5557
0	0.113	3.45	69	69	3862

WDC	CSAFR	DMR	σ_3	σ_d	M_R
0	0.113	3.45	69	138	3892
0	0.113	3.45	69	208	3996
0	0.113	3.45	69	277	5151
0	0.113	3.45	34.5	69	3762
0	0.113	3.45	34.5	138	3842
0	0.113	3.45	34.5	208	3944
0	0.113	3.45	34.5	277	5110
0	0.113	3.45	0	69	3803
0	0.113	3.45	0	138	3813
0	0.113	3.45	0	208	3838
0	0.113	3.45	0	277	4998
0	0.510	2.61	138	69	4500
0	0.510	2.61	138	138	4761
0	0.510	2.61	138	208	5039
0	0.510	2.61	138	277	6290
0	0.510	2.61	103.5	69	4502
0	0.510	2.61	103.5	138	4502
0	0.510	2.61	103.5	208	4732
0	0.510	2.61	103.5	277	6289
0	0.510	2.61	69	69	4488
0	0.510	2.61	69	138	4619
0	0.510	2.61	69	208	4700
0	0.510	2.61	69	277	6290
0	0.510	2.61	34.5	69	4445
0	0.510	2.61	34.5	138	4589
0	0.510	2.61	34.5	208	4746
0	0.510	2.61	34.5	277	5620
0	0.510	2.61	0	69	4438
0	0.510	2.61	0	138	4553
0	0.510	2.61	0	208	4726
0	0.510	2.61	0	277	5575
0	0.510	4.63	138	69	8691
0	0.510	4.63	138	138	8838
0	0.510	4.63	138	208	9062
0	0.510	4.63	103.5	69	8798
0	0.510	4.63	103.5	138	8956
0	0.510	4.63	103.5	208	9404
0	0.510	4.63	69	69	8832
0	0.510	4.63	69	138	9120
0	0.510	4.63	69	208	9788
0	0.510	4.63	34.5	69	8880
0	0.510	4.63	34.5	138	9142
0	0.510	4.63	34.5	208	9665
0	0.510	4.63	0	69	8900
0	0.510	4.63	0	138	9205
0	0.510	4.63	0	208	9803
0	0.510	3.89	138	69	4146
0	0.510	3.89	138	138	4617
0	0.510	3.89	138	208	4988
0	0.510	3.89	138	277	5222
0	0.510	3.89	103.5	69	4119
0	0.510	3.89	103.5	138	4306
0	0.510	3.89	103.5	208	4588
0	0.510	3.89	103.5	277	5002
0	0.510	3.89	69	69	4113
0	0.510	3.89	69	138	4254
0	0.510	3.89	69	208	4505

WDC	CSAFR	DMR	σ_3	σ_d	M_R
0	0.510	3.89	69	277	5344
0	0.510	3.89	34.5	69	4128
0	0.510	3.89	34.5	138	4236
0	0.510	3.89	34.5	208	4541
0	0.510	3.89	34.5	277	5241
0	0.510	3.89	0	69	4133
0	0.510	3.89	0	138	4204
0	0.510	3.89	0	208	4492
0	0.510	3.89	0	277	5358
0	0.510	3.37	138	69	3440
0	0.510	3.37	138	138	3786
0	0.510	3.37	138	208	4129
0	0.510	3.37	138	277	4464
0	0.510	3.37	103.5	69	3392
0	0.510	3.37	103.5	138	3434
0	0.510	3.37	103.5	208	3525
0	0.510	3.37	103.5	277	3821
0	0.510	3.37	69	69	3405
0	0.510	3.37	69	138	3426
0	0.510	3.37	69	208	3455
0	0.510	3.37	69	277	3821
0	0.510	3.37	34.5	69	3362
0	0.510	3.37	34.5	138	3392
0	0.510	3.37	34.5	208	3476
0	0.510	3.37	34.5	277	3751
0	0.510	3.37	0	69	3392
0	0.510	3.37	0	138	3427
0	0.510	3.37	0	208	3503
0	0.510	3.37	0	277	3749
8	0.130	2.34	138	69	1299
8	0.130	2.34	138	138	1458
8	0.130	2.34	138	208	1550
8	0.130	2.34	138	277	1721
8	0.130	2.34	103.5	69	1363
8	0.130	2.34	103.5	138	1364
8	0.130	2.34	103.5	208	1386
8	0.130	2.34	103.5	277	1489
8	0.130	2.34	69	69	1272
8	0.130	2.34	69	138	1307
8	0.130	2.34	69	208	1346
8	0.130	2.34	69	277	1403
8	0.130	2.34	34.5	69	1252
8	0.130	2.34	34.5	138	1279
8	0.130	2.34	34.5	208	1331
8	0.130	2.34	34.5	277	1375
8	0.130	2.34	0	69	1229
8	0.130	2.34	0	138	1260
8	0.130	2.34	0	208	1315
8	0.130	2.34	0	277	1358
8	0.130	3.43	138	69	4062
8	0.130	3.43	138	138	4248
8	0.130	3.43	138	208	4625
8	0.130	3.43	138	277	5003
8	0.130	3.43	103.5	69	3877
8	0.130	3.43	103.5	138	3992
8	0.130	3.43	103.5	208	4357
8	0.130	3.43	103.5	277	4792

WDC	CSAFR	DMR	σ_3	σ_d	M_R
8	0.130	3.43	69	69	3929
8	0.130	3.43	69	138	3931
8	0.130	3.43	69	208	4194
8	0.130	3.43	69	277	4650
8	0.130	3.43	34.5	69	3648
8	0.130	3.43	34.5	138	3656
8	0.130	3.43	34.5	208	3704
8	0.130	3.43	34.5	277	4210
8	0.130	3.43	0	69	3527
8	0.130	3.43	0	138	3732
8	0.130	3.43	0	208	3763
8	0.130	3.43	0	277	4737
8	0.130	2.84	138	69	4278
8	0.130	2.84	138	138	4537
8	0.130	2.84	138	208	5232
8	0.130	2.84	138	277	6069
8	0.130	2.84	103.5	69	4163
8	0.130	2.84	103.5	138	4354
8	0.130	2.84	103.5	208	4987
8	0.130	2.84	103.5	277	5617
8	0.130	2.84	69	69	4202
8	0.130	2.84	69	138	4291
8	0.130	2.84	69	208	4653
8	0.130	2.84	69	277	5374
8	0.130	2.84	34.5	69	4348
8	0.130	2.84	34.5	138	4668
8	0.130	2.84	34.5	208	4754
8	0.130	2.84	34.5	277	5252
8	0.130	2.84	0	69	4105
8	0.130	2.84	0	208	4812
8	0.130	2.84	0	277	5278
8	0.130	2.48	138	69	2179
8	0.130	2.48	138	138	2328
8	0.130	2.48	138	208	2524
8	0.130	2.48	138	277	2752
8	0.130	2.48	103.5	69	2124
8	0.130	2.48	103.5	138	2154
8	0.130	2.48	103.5	208	2155
8	0.130	2.48	103.5	277	2425
8	0.130	2.48	69	69	2032
8	0.130	2.48	69	138	2049
8	0.130	2.48	69	208	2074
8	0.130	2.48	69	277	2194
8	0.130	2.48	34.5	69	2014
8	0.130	2.48	34.5	138	2029
8	0.130	2.48	34.5	208	2075
8	0.130	2.48	34.5	277	2193
8	0.130	2.48	0	69	1947
8	0.130	2.48	0	138	1958
8	0.130	2.48	0	208	2020
8	0.130	2.48	0	277	2195
8	0.113	4.08	138	69	4043
8	0.113	4.08	138	138	4632
8	0.113	4.08	138	208	5129
8	0.113	4.08	138	277	6125
8	0.113	4.08	103.5	69	4042
8	0.113	4.08	103.5	138	4174

WDC	CSAFR	DMR	σ_3	σ_d	M_R
8	0.113	4.08	103.5	208	4328
8	0.113	4.08	103.5	277	5200
8	0.113	4.08	69	69	4054
8	0.113	4.08	69	138	4102
8	0.113	4.08	69	208	4222
8	0.113	4.08	69	277	4836
8	0.113	4.08	34.5	69	4067
8	0.113	4.08	34.5	138	4211
8	0.113	4.08	34.5	208	4263
8	0.113	4.08	34.5	277	4912
8	0.113	4.08	0	69	4047
8	0.113	4.08	0	138	4081
8	0.113	4.08	0	208	4242
8	0.113	4.08	0	277	5180
8	0.113	3.45	138	69	3248
8	0.113	3.45	138	138	3656
8	0.113	3.45	138	208	4535
8	0.113	3.45	138	277	5263
8	0.113	3.45	103.5	69	3222
8	0.113	3.45	103.5	138	2965
8	0.113	3.45	103.5	208	3066
8	0.113	3.45	103.5	277	3190
8	0.113	3.45	69	69	2934
8	0.113	3.45	69	138	2832
8	0.113	3.45	69	208	2951
8	0.113	3.45	69	277	3145
8	0.113	3.45	34.5	69	2871
8	0.113	3.45	34.5	138	2748
8	0.113	3.45	34.5	208	2924
8	0.113	3.45	34.5	277	3111
8	0.113	3.45	0	69	2742
8	0.113	3.45	0	138	2712
8	0.113	3.45	0	208	2902
8	0.113	3.45	0	277	3097
8	0.510	2.61	138	69	4538
8	0.510	2.61	138	138	5462
8	0.510	2.61	138	208	6157
8	0.510	2.61	138	277	6658
8	0.510	2.61	103.5	69	3948
8	0.510	2.61	103.5	138	3951
8	0.510	2.61	103.5	208	4193
8	0.510	2.61	103.5	277	4297
8	0.510	2.61	69	69	3581
8	0.510	2.61	69	138	3639
8	0.510	2.61	69	208	3942
8	0.510	2.61	69	277	4174
8	0.510	2.61	34.5	69	3456
8	0.510	2.61	34.5	138	3518
8	0.510	2.61	34.5	208	3824
8	0.510	2.61	34.5	277	4100
8	0.510	2.61	0	69	3371
8	0.510	2.61	0	138	3427
8	0.510	2.61	0	208	3768
8	0.510	2.61	0	277	4110
8	0.510	4.63	138	69	7979
8	0.510	4.63	138	138	8253
8	0.510	4.63	138	208	8658

WDC	CSAFR	DMR	σ_3	σ_d	M_R
8	0.510	4.63	138	277	9318
8	0.510	4.63	103.5	69	7414
8	0.510	4.63	103.5	138	8253
8	0.510	4.63	103.5	208	8708
8	0.510	4.63	103.5	277	9306
8	0.510	4.63	69	69	7601
8	0.510	4.63	69	138	8378
8	0.510	4.63	69	208	8923
8	0.510	4.63	69	277	9321
8	0.510	4.63	34.5	69	8101
8	0.510	4.63	34.5	138	8196
8	0.510	4.63	34.5	208	9101
8	0.510	4.63	34.5	277	9591
8	0.510	4.63	0	69	8055
8	0.510	4.63	0	138	8307
8	0.510	4.63	0	208	8915
8	0.510	4.63	0	277	9644
8	0.510	3.89	138	69	3091
8	0.510	3.89	138	138	3358
8	0.510	3.89	138	208	3745
8	0.510	3.89	138	277	4055
8	0.510	3.89	103.5	69	2953
8	0.510	3.89	103.5	138	2765
8	0.510	3.89	69	69	2459
8	0.510	3.37	138	69	2902
8	0.510	3.37	138	138	2924
8	0.510	3.37	138	208	3060
8	0.510	3.37	138	277	3193
8	0.510	3.37	103.5	69	2496
8	0.510	3.37	103.5	138	2595
8	0.510	3.37	103.5	208	2917
8	0.510	3.37	103.5	277	3180
8	0.510	3.37	69	69	2364
8	0.510	3.37	69	138	2549
8	0.510	3.37	69	208	2881
8	0.510	3.37	69	277	3160
8	0.510	3.37	34.5	69	2382
8	0.510	3.37	34.5	138	2530
8	0.510	3.37	34.5	208	2885
8	0.510	3.37	34.5	277	3205
8	0.510	3.37	0	69	2437
8	0.510	3.37	0	138	2658
8	0.510	3.37	0	208	2945
8	0.510	3.37	0	277	3278
16	0.130	2.34	138	69	1071
16	0.130	2.34	138	138	1183
16	0.130	2.34	138	208	1260
16	0.130	2.34	138	277	1405
16	0.130	2.34	103.5	69	1039
16	0.130	2.34	103.5	138	1041
16	0.130	2.34	103.5	208	1081
16	0.130	2.34	103.5	277	1384
16	0.130	2.34	69	69	1008
16	0.130	2.34	69	138	1018
16	0.130	2.34	69	208	1033
16	0.130	2.34	69	277	1277
16	0.130	2.34	34.5	69	985

WDC	CSAFR	DMR	σ_3	σ_d	M_R
16	0.130	2.34	34.5	138	994
16	0.130	2.34	34.5	208	1006
16	0.130	2.34	34.5	277	1195
16	0.130	2.34	0	69	960
16	0.130	2.34	0	138	969
16	0.130	2.34	0	208	989
16	0.130	2.34	0	277	1151
16	0.130	3.43	138	69	3012
16	0.130	3.43	138	138	3530
16	0.130	3.43	138	208	5466
16	0.130	3.43	138	277	5970
16	0.130	3.43	103.5	69	3377
16	0.130	3.43	103.5	138	3017
16	0.130	3.43	103.5	208	3564
16	0.130	3.43	103.5	277	2957
16	0.130	3.43	69	69	3250
16	0.130	3.43	69	138	2916
16	0.130	3.43	69	208	3559
16	0.130	3.43	69	277	2941
16	0.130	3.43	34.5	69	3408
16	0.130	3.43	34.5	138	3443
16	0.130	3.43	34.5	208	2971
16	0.130	3.43	34.5	277	2943
16	0.130	3.43	0	69	3299
16	0.130	3.43	0	138	3334
16	0.130	3.43	0	208	2904
16	0.130	3.43	0	277	2897
16	0.130	2.84	138	69	3295
16	0.130	2.84	138	138	3612
16	0.130	2.84	138	208	4178
16	0.130	2.84	138	277	4184
16	0.130	2.84	103.5	69	3346
16	0.130	2.84	103.5	138	3552
16	0.130	2.84	103.5	208	4550
16	0.130	2.84	103.5	277	5002
16	0.130	2.84	69	69	3430
16	0.130	2.84	69	138	3606
16	0.130	2.84	69	277	4972
16	0.130	2.84	34.5	69	3427
16	0.130	2.84	34.5	138	3598
16	0.130	2.84	0	69	3590
16	0.130	2.84	0	138	3597
16	0.130	2.48	138	69	1618
16	0.130	2.48	138	138	1798
16	0.130	2.48	138	208	2102
16	0.130	2.48	138	277	2991
16	0.130	2.48	103.5	69	1595
16	0.130	2.48	103.5	138	1638
16	0.130	2.48	103.5	208	1749
16	0.130	2.48	103.5	277	2273
16	0.130	2.48	69	69	1565
16	0.130	2.48	69	138	1603
16	0.130	2.48	69	208	1666
16	0.130	2.48	69	277	2201
16	0.130	2.48	34.5	69	1558
16	0.130	2.48	34.5	138	1574
16	0.130	2.48	34.5	208	1656

WDC	CSAFR	DMR	σ_3	σ_d	M_R
16	0.130	2.48	34.5	277	2111
16	0.130	2.48	0	69	1543
16	0.130	2.48	0	138	1550
16	0.130	2.48	0	208	1634
16	0.130	2.48	0	277	2068
16	0.113	4.08	138	69	3576
16	0.113	4.08	138	138	3855
16	0.113	4.08	138	208	4246
16	0.113	4.08	138	277	4391
16	0.113	4.08	103.5	69	3470
16	0.113	4.08	103.5	138	3700
16	0.113	4.08	103.5	208	4193
16	0.113	4.08	103.5	277	4473
16	0.113	4.08	69	69	3471
16	0.113	4.08	69	138	3767
16	0.113	4.08	69	208	4237
16	0.113	4.08	69	277	4522
16	0.113	4.08	34.5	69	3418
16	0.113	4.08	34.5	138	3779
16	0.113	4.08	34.5	208	4179
16	0.113	4.08	34.5	277	4475
16	0.113	4.08	0	69	3389
16	0.113	4.08	0	138	3819
16	0.113	4.08	0	208	4067
16	0.113	4.08	0	277	4469
16	0.113	3.45	138	69	2596
16	0.113	3.45	138	138	2898
16	0.113	3.45	138	208	2908
16	0.113	3.45	138	277	3006
16	0.113	3.45	103.5	69	1901
16	0.113	3.45	103.5	138	2164
16	0.113	3.45	103.5	208	2582
16	0.113	3.45	103.5	277	2936
16	0.113	3.45	69	69	1766
16	0.113	3.45	69	138	2094
16	0.113	3.45	69	208	2483
16	0.113	3.45	69	277	2886
16	0.113	3.45	34.5	69	1683
16	0.113	3.45	34.5	138	2043
16	0.113	3.45	34.5	208	2433
16	0.113	3.45	34.5	277	2808
16	0.113	3.45	0	69	1537
16	0.113	3.45	0	138	1895
16	0.113	3.45	0	208	2305
16	0.113	3.45	0	277	2709
16	0.510	2.61	138	69	4057
16	0.510	2.61	138	138	4511
16	0.510	2.61	138	208	5210
16	0.510	2.61	138	277	5575
16	0.510	2.61	103.5	69	3531
16	0.510	2.61	103.5	138	3525
16	0.510	2.61	103.5	208	3735
16	0.510	2.61	103.5	277	3861
16	0.510	2.61	69	69	3182
16	0.510	2.61	69	138	3307
16	0.510	2.61	69	208	3550
16	0.510	2.61	69	277	3753

WDC	CSAFR	DMR	σ_3	σ_d	M_R
16	0.510	2.61	34.5	69	3115
16	0.510	2.61	34.5	138	3183
16	0.510	2.61	34.5	208	3464
16	0.510	2.61	34.5	277	3708
16	0.510	2.61	0	69	3022
16	0.510	2.61	0	138	3136
16	0.510	2.61	0	208	3437
16	0.510	2.61	0	277	3696
16	0.510	4.63	138	69	5124
16	0.510	4.63	138	138	5984
16	0.510	4.63	138	208	7128
16	0.510	4.63	138	277	9058
16	0.510	4.63	103.5	69	5174
16	0.510	4.63	103.5	138	5761
16	0.510	4.63	103.5	208	7290
16	0.510	4.63	103.5	277	8780
16	0.510	4.63	69	69	5247
16	0.510	4.63	69	138	5859
16	0.510	4.63	69	208	7304
16	0.510	4.63	69	277	8540
16	0.510	4.63	34.5	69	5408
16	0.510	4.63	34.5	138	5971
16	0.510	4.63	34.5	208	7279
16	0.510	4.63	34.5	277	8358
16	0.510	4.63	0	69	5473
16	0.510	4.63	0	138	6107
16	0.510	4.63	0	208	8289
16	0.510	4.63	0	277	9448
30	0.130	2.34	138	69	935
30	0.130	2.34	138	138	935
30	0.130	2.34	138	208	965
30	0.130	2.34	138	277	1019
30	0.130	2.34	103.5	208	835
30	0.130	2.34	103.5	277	894
30	0.130	2.34	34.5	69	603
30	0.130	2.34	34.5	208	773
30	0.130	2.34	34.5	277	846
30	0.130	2.34	0	69	585
30	0.130	2.34	0	138	666
30	0.130	2.34	0	208	757
30	0.130	2.34	0	277	838
30	0.130	3.43	138	69	3322
30	0.130	3.43	138	138	3315
30	0.130	3.43	138	208	3547
30	0.130	3.43	138	277	3556
30	0.130	3.43	103.5	69	2632
30	0.130	3.43	103.5	138	2787
30	0.130	3.43	103.5	208	3043
30	0.130	3.43	103.5	277	3300
30	0.130	3.43	69	69	2557
30	0.130	3.43	69	138	2762
30	0.130	3.43	69	208	2993
30	0.130	3.43	69	277	3284
30	0.130	3.43	34.5	69	2517

Table A1. Training dataset used in LSTM modeling.

WDC	CSAFR	DMR	σ_3	σ_d	M_R
30	0.130	3.43	34.5	138	2765
30	0.130	3.43	34.5	208	2965
30	0.130	3.43	34.5	277	3257
30	0.130	3.43	0	69	2453
30	0.130	3.43	0	138	2739
30	0.130	3.43	0	208	2943
30	0.130	3.43	0	277	3239
30	0.130	2.84	138	69	2812
30	0.130	2.84	138	138	2938
30	0.130	2.84	138	208	3765
30	0.130	2.84	138	277	4355
30	0.130	2.84	103.5	69	3038
30	0.130	2.84	103.5	138	2775
30	0.130	2.84	103.5	208	3465
30	0.130	2.84	103.5	277	2782
30	0.130	2.84	69	69	2961
30	0.130	2.84	69	138	2721
30	0.130	2.84	69	208	3321
30	0.130	2.84	69	277	2741
30	0.130	2.84	34.5	69	2665
30	0.130	2.84	34.5	138	3275
30	0.130	2.84	34.5	208	2683
30	0.130	2.84	34.5	277	2714
30	0.130	2.84	0	69	2597
30	0.130	2.84	0	208	2660
30	0.130	2.84	0	277	2692
30	0.130	2.48	138	69	1519
30	0.130	2.48	138	138	1672
30	0.130	2.48	138	208	1735
30	0.130	2.48	138	277	1823
30	0.130	2.48	103.5	69	1468
30	0.130	2.48	103.5	138	1484
30	0.130	2.48	103.5	208	1554
30	0.130	2.48	103.5	277	1574
30	0.130	2.48	69	69	1421
30	0.130	2.48	69	138	1457
30	0.130	2.48	69	208	1478
30	0.130	2.48	69	277	1533
30	0.130	2.48	34.5	69	1392
30	0.130	2.48	34.5	138	1435
30	0.130	2.48	34.5	208	1438
30	0.130	2.48	34.5	277	1506
30	0.130	2.48	0	69	1373
30	0.130	2.48	0	138	1411
30	0.130	2.48	0	208	1421
30	0.130	2.48	0	277	1458
30	0.113	4.08	138	69	3599
30	0.113	4.08	138	138	3619
30	0.113	4.08	138	208	3705
30	0.113	4.08	138	277	3867
30	0.113	4.08	103.5	69	3059
30	0.113	4.08	103.5	138	3406
30	0.113	4.08	103.5	208	3654
30	0.113	4.08	103.5	277	3939
30	0.113	4.08	69	69	3108
30	0.113	4.08	69	138	3364

WDC	CSAFR	DMR	σ_3	σ_d	M_R
30	0.113	4.08	69	208	3637
30	0.113	4.08	69	277	3913
30	0.113	4.08	34.5	69	3049
30	0.113	4.08	34.5	138	3422
30	0.113	4.08	34.5	208	3711
30	0.113	4.08	34.5	277	3869
30	0.113	4.08	0	69	2987
30	0.113	4.08	0	138	3338
30	0.113	4.08	0	208	3684
30	0.113	4.08	0	277	3975
30	0.113	3.45	138	69	2291
30	0.113	3.45	138	138	2249
30	0.113	3.45	138	208	2465
30	0.113	3.45	138	277	2537
30	0.113	3.45	103.5	69	1981
30	0.113	3.45	103.5	138	1955
30	0.113	3.45	103.5	208	2089
30	0.113	3.45	103.5	277	2197
30	0.113	3.45	69	69	1927
30	0.113	3.45	69	138	1914
30	0.113	3.45	69	208	2043
30	0.113	3.45	69	277	2160
30	0.113	3.45	34.5	69	1872
30	0.113	3.45	34.5	138	1871
30	0.113	3.45	34.5	208	1998
30	0.113	3.45	34.5	277	2126
30	0.113	3.45	0	69	1827
30	0.113	3.45	0	138	1867
30	0.113	3.45	0	208	1977
30	0.113	3.45	0	277	2127
30	0.510	2.61	138	69	3493
30	0.510	2.61	138	138	3647
30	0.510	2.61	138	208	4118
30	0.510	2.61	103.5	69	3166
30	0.510	2.61	103.5	138	2714
30	0.510	2.61	103.5	208	3001
30	0.510	2.61	103.5	277	3330
30	0.510	2.61	69	69	2876
30	0.510	2.61	69	138	2532
30	0.510	2.61	69	208	2846
30	0.510	2.61	69	277	3240
30	0.510	2.61	34.5	69	2820
30	0.510	2.61	34.5	138	2428
30	0.510	2.61	34.5	208	2775
30	0.510	2.61	34.5	277	3202
30	0.510	2.61	0	69	2742
30	0.510	2.61	0	138	2389
30	0.510	2.61	0	208	2753
30	0.510	2.61	0	277	3192
30	0.510	4.4	138	69	5461
30	0.510	4.4	138	138	5675
30	0.510	4.4	138	208	6251
30	0.510	4.4	138	277	7617
30	0.510	4.4	103.5	69	5427
30	0.510	4.4	103.5	138	5709
30	0.510	4.4	103.5	208	6247
30	0.510	4.4	103.5	277	7591

WDC	CSAFR	DMR	σ_3	σ_d	M_R
30	0.510	4.4	69	69	5485
30	0.510	4.4	69	138	5685
30	0.510	4.4	69	208	6248
30	0.510	4.4	69	277	7203
30	0.510	4.4	34.5	69	5454
30	0.510	4.4	34.5	138	5732
30	0.510	4.4	34.5	208	6189
30	0.510	4.4	34.5	277	7435
30	0.510	4.4	0	69	5400
30	0.510	4.4	0	138	5564
30	0.510	4.4	0	208	5894
30	0.510	4.4	0	277	7283
30	0.510	3.37	138	69	2504
30	0.510	3.37	138	138	2624
30	0.510	3.37	138	208	2418
30	0.510	3.37	138	277	2517
30	0.510	3.37	103.5	69	1814
30	0.510	3.37	103.5	138	2009
30	0.510	3.37	103.5	208	2227
30	0.510	3.37	103.5	277	2340
30	0.510	3.37	69	69	1724
30	0.510	3.37	69	138	1883
30	0.510	3.37	69	208	2090
30	0.510	3.37	69	277	2302
30	0.510	3.37	34.5	69	1694
30	0.510	3.37	34.5	138	1846
30	0.510	3.37	34.5	208	2043
30	0.510	3.37	34.5	277	2250
30	0.510	3.37	0	277	1632

Table A2. Testing dataset used in LSTM model validation.

Received: 8 August 2024; Accepted: 11 November 2024
Published online: 13 November 2024

References

1. Kaloop, M. R. et al. Particle swarm optimization algorithm-extreme learning machine (PSO-ELM) model for predicting resilient modulus of stabilized aggregate bases, Applied Sciences, **9**, 16, p. 3221, (2019).
2. Sas, W., Gluchowski, A. & Szymanski, A. Determination of the Resilient modulus MR for the lime stabilized clay obtained from the repeated loading CBR tests, Annals of Warsaw University of Life Sciences-SGGW. Land Reclamation, vol. 44, no. 2, (2012).
3. Barksdale, R. D. et al. Laboratory determination of resilient modulus for flexible pavement design, (1997).
4. Khoury, N. & Zaman, M. M. Durability of stabilized base courses subjected to wet–dry cycles. *Int. J. Pavement Eng.* **8** (4), 265–276 (2007).
5. AASHTO. AASHTO Guide for Design of Pavement Structures. (1993).
6. Zaman, M., Solanki, P., Ebrahimi, A. & White, L. Neural network modeling of resilient modulus using routine subgrade soil properties. *Int. J. Geomech.* **10** (1), 1–12 (2010).
7. Wang, H., Zhang, X. & Jiang, S. J. S. A laboratory and field universal estimation method for tire–pavement interaction noise (TPIN) based on 3D image technology, vol. 14, no. 19, p. 12066, (2022).
8. Erlingsson, S. & Rahman, M. S. Evaluation of permanent deformation characteristics of unbound granular materials by means of multistage repeated-load triaxial tests. *Transp. Res. Rec.* **2369** (1), 11–19 (2013).
9. Hossain, M. S. & Kim, W. S. Estimation of subgrade resilient modulus for fine-grained soil from unconfined compression test. *Transp. Res. Rec.* **2473** (1), 126–135 (2015).
10. Fedrigo, W., Núñez, W. P., López, M. A. C., Kleinert, T. R. & Ceratti, J. A. P. A study on the resilient modulus of cement-treated mixtures of RAP and aggregates using indirect tensile, triaxial and flexural tests. *Constr. Build. Mater.* **171**, 161–169 (2018).
11. Putri, E. E., Rao, N. & Mannan, M. Evaluation of the modulus of elasticity and resilient modulus for highway subgrades. *Electron. J. Geotech. Eng.* **15**, 1285–1293 (2010).
12. Zhou, F., Hu, S., Chen, D. H. & Scullion, T. Overlay tester: simple performance test for fatigue cracking, Transportation Research Record, vol. no. 1, pp. 1–8, 2007. (2001).
13. Radhakrishnan, V., Dudipala, R. R., Maity, A. & Sudhakar Reddy, K. Evaluation of rutting potential of asphalts using resilient modulus test parameters. *Road. Mater. Pavement Des.* **20** (1), 20–35 (2019).
14. Loulizi, A., Flintsch, G. W., Al-Qadi, I. L. & Mokarem, D. Comparing resilient modulus and dynamic modulus of hot-mix asphalt as material properties for flexible pavement design, Transportation Research Record, vol. no. 1, pp. 161–170, 2006. (1970).
15. Khan, K. et al. Prediction Models for Evaluating Resilient Modulus of Stabilized Aggregate Bases in Wet and Dry Alternating Environments: ANN and GEP Approaches, Materials, vol. 15, no. 13, p. 4386, (2022).

16. Olidis, C. & Hein, D. Guide for the mechanistic-empirical design of new and rehabilitated pavement structures materials characterization: Is your agency ready, in 2004 annual conference of the transportation association of Canada, (2004).
17. Berg, K. Durability and strength of activated reclaimed Iowa Class C fly ash aggregate in road bases, 1998.
18. Nunan, T. A. & Humphrey, D. *A REVIEW AND EXPERIMENTATION OF GRAVEL STABILIZATION METHODS* (EXECUTIVE SUMMARY, 1990).
19. Zaman, M. M., Zhu, J. H. & Laguros, J. G. Durability effects on resilient moduli of stabilized aggregate base. *Transp. Res. Rec.* **1687** (1), 29–38 (1999).
20. Guthrie, W. S., Michener, J. E., Wilson, B. T. & Eggett, D. L. Effects of environmental factors on construction of soil–cement pavement layers, Transportation research record, **2104**, 1, pp. 71–79, (2009).
21. Khoury, N. N. *Durability of Cementitiously Stabilized Aggregate Bases for Pavement Application* (The University of Oklahoma, 2005).
22. George, K. P. & Davidson, D. T. Development of a freeze-thaw test for design of soil-cement. *Highway Res. Record no* 36, (1963).
23. Butalia, T. S., Huang, J., Kim, D. G. & Croft, F. Effect of moisture content and pore water pressure buildup on resilient modulus of cohesive soils in Ohio, ASTM Special Technical Publication, **1437**, pp. 70–84, (2003).
24. Khoury, N. N. & Zaman, M. M. Correlation between resilient modulus, moisture variation, and soil suction for subgrade soils, Transportation research record, vol. 1874, no. 1, pp. 99–107, (2004).
25. Diagne, M., Tinjum, J. M. & Nokkaew, K. The effects of recycled clay brick content on the engineering properties, weathering durability, and resilient modulus of recycled concrete aggregate, Transportation Geotechnics, **3**, pp. 15–23, (2015).
26. Khoury, N., Brooks, R., Boeni, S. Y. & Yada, D. Variation of resilient modulus, strength, and modulus of elasticity of stabilized soils with postcompaction moisture contents. *J. Mater. Civ. Eng.* **25** (2), 160–166 (2013).
27. Khoury, N. N. & Brooks, R. Performance of a stabilized aggregate base subject to different durability procedures. *J. Mater. Civ. Eng.* **22** (5), 506–514 (2010).
28. Ahmad, M. et al. Application of machine learning algorithms for the evaluation of seismic soil liquefaction potential, vol. 15, pp. 490–505, (2021).
29. Ahmad, M. et al. Prediction of liquefaction-induced lateral displacements using Gaussian process regression, vol. 12, no. 4, p. 2022. (1977).
30. Ahmad, F. et al. Prediction of slope stability using Tree Augmented Naive-Bayes classifier: Modeling and performance evaluation, vol. 19, no. 5, pp. 4526–4546, (2022).
31. Ahmad, F., Tang, X., Hu, J., Ahmad, M. & Gordan, B. J. Improved Prediction of Slope Stability under Static and Dynamic Conditions Using Tree-Based Models, vol. 1, p. 3, (2023).
32. Ahmad, F. et al. Stability risk assessment of slopes using logistic model tree based on updated case histories, **20**, 12, pp. 21229–21245, (2023).
33. Ahmad, M. et al. Unconfined compressive strength prediction of stabilized expansive clay soil using machine learning techniques, pp. 1–15, (2023).
34. Barkhordari, M. S., Barkhordari, M. M., Armaghani, D. J., Mohamad, E. T. & Gordan, B. Straightforward slope stability prediction under seismic conditions using machine learning algorithms, (2023).
35. Asteris, P. G. et al. Slope stability classification under seismic conditions using several tree-based intelligent techniques, vol. 12, no. 3, p. 1753, (2022).
36. Li, D., Liu, Z., Armaghani, D. J., Xiao, P. & Zhou, J. J. M. Novel ensemble tree solution for rockburst prediction using deep forest, vol. 10, no. 5, p. 787, (2022).
37. Armaghani, D. J., Hajihassani, M., Mohamad, E. T. & Marto, A. and S. J. A. J. o. G. Noorani, blasting-induced flyrock and ground vibration prediction through an expert artificial neural network based on particle swarm optimization, **7**, pp. 5383–5396, (2014).
38. Armaghani, D. J. et al. Development of hybrid intelligent models for predicting TBM penetration rate in hard rock condition, vol. 63, pp. 29–43, (2017).
39. Hu, D. et al. Surface Settlement Prediction of Rectangular Pipe-Jacking Tunnel Based on the Machine-Learning Algorithm, vol. 15, no. 1, p. 04023061, (2024).
40. Gu, X., Chen, X., Lu, P., Lan, X. & Li, X. and Y. J. T. J. o. S. Du, SiMaLSTM-SNP: novel semantic relatedness learning model preserving both Siamese networks and membrane computing, vol. 80, no. 3, pp. 3382–3411, (2024).
41. Karballaeezadeh, N. et al. Intelligent road inspection with advanced machine learning; hybrid prediction models for smart mobility and transportation maintenance systems, vol. 13, no. 7, p. 1718, (2020).
42. Jalali, H. et al. Prediction of vertical displacement for a buried pipeline subjected to normal fault using a hybrid FEM-ANN approach, pp. 1–16, (2024).
43. Maalouf, M., Khoury, N., Laguros, J. G. & Kumin, H. Support vector regression to predict the performance of stabilized aggregate bases subject to wet–dry cycles, International journal for numerical and analytical methods in geomechanics, **36**, 6, pp. 675–696, (2012).
44. Maalouf, M. & Homouz, D. Kernel ridge regression using truncated newton method. *Knowl. Based Syst.* **71**, 339–344 (2014).
45. Ghanizadeh, A. & Rahrovan, M. Application of artifitial neural network to predict the resilient modulus of stabilized base subjected to wet dry cycles. *Comput. Mater. Civ. Eng.* **1**, 37–47 (2016).
46. Ghanizadeh, A., Tavana, A., Amlashi & Abbasou, H. Prediction of Resilient Modulus of Stabilized Aggregate Base Subjected To Wet-Dry Cycles Using Adaptive Neuro-Fuzzy Inference System (ANFIS), Road, vol. 25, no. 90, pp. 65–75, (2017).
47. Ghanizadeh, A. R., Heidarabadizadeh, N. & Heravi, F. Gaussian process regression (gpr) for auto-estimation of resilient modulus of stabilized base materials. *J. Soft Comput. Civil Eng.* **5** (1), 80–94 (2021).
48. Khoury, N., I. J., M. J. & Zaman, P. E. Influences of various cementitious agents on the performance of stabilized aggregate base subjected to wet-dry cycles, **8**, 4, pp. 265–276, (2007).
49. Ren, L. et al. A data-driven auto-CNN-LSTM prediction model for lithium-ion battery remaining useful life. *IEEE Trans. Industr. Inf.* **17** (5), 3478–3487 (2020).
50. Gers, F. A., Schmidhuber, J. & Cummins, F. Learning to forget: Continual prediction with LSTM, Neural computation, vol. 12, no. 10, pp. 2451–2471, (2000).
51. Chen, K., Zhou, Y. & Dai, F. A LSTM-based method for stock returns prediction: A case study of China stock market, in 2015 IEEE international conference on big data (big data), pp. 2823–2824: IEEE. (2015).
52. Wang, J., Li, J., Wang, X., Wang, J. & Huang, M. Air quality prediction using CT-LSTM. *Neural Comput. Appl.* **33**, 4779–4792 (2021).
53. Alhirmizy, S. & Qader, B. Multivariate time series forecasting with LSTM for Madrid, Spain pollution, in 2019 international conference on computing and information science and technology and their applications (ICCISTA), pp. 1–5: IEEE. (2019).
54. Schmidhuber, J., Gers, F. & Eck, D. Learning nonregular languages: a comparison of simple recurrent networks and LSTM, neural computation, **14**, 9, pp. 2039–2041, (2002).
55. Hochreiter, S. & Schmidhuber, J. Long short-term memory, neural computation, **9**, 8, pp. 1735–1780, (1997).
56. Sherstinsky, A. Fundamentals of recurrent neural network (RNN) and long short-term memory (LSTM) network. *Phys. D: Nonlinear Phenom.* **404**, 132306 (2020).
57. Asteris, P. G., Koopialipoor, M., Armaghani, D. J., Kotsonis, E. A. & Lourenço, P. B. Prediction of cement-based mortars compressive strength using machine learning techniques. *Neural Comput. Appl.* **33** (19), 13089–13121 (2021).

58. Ly, H. B. et al. Estimation of axial load-carrying capacity of concrete-filled steel tubes using surrogate models. *Neural Comput. Appl.* **33** (8), 3437–3458 (2021).
59. Asteris, P. G., Skentou, A. D., Bardhan, A., Samui, P. & Lourenço, P. B. Soft computing techniques for the prediction of concrete compressive strength using non-destructive tests. *Constr. Build. Mater.* **303**, 124450 (2021).
60. Asteris, P. G., Lemonis, M. E., Le, T. T. & Tsavdaridis, K. D. Evaluation of the ultimate eccentric load of rectangular CFSTs using advanced neural network modeling. *Eng. Struct.* **248**, 113297 (2021).
61. Arora, H. C. et al. Axial Capacity of FRP-Reinforced Concrete Columns: Computational Intelligence-Based Prognosis for Sustainable Structures, Buildings, vol. 12, no. 12, p. 2137, (2022).
62. Gandomi, A. H., Babanajad, S. K., Alavi, A. H. & Farnam, Y. Novel approach to strength modeling of concrete under triaxial compression. *J. Mater. Civ. Eng.* **24** (9), 1132–1143 (2012).
63. Bui, X. N. et al. Prediction of slope failure in open-pit mines using a novel hybrid artificial intelligence model based on decision tree and evolution algorithm, scientific reports, **10**, 1, pp. 1–17, (2020).
64. Manouchehrian, A., Gholamnejad, J. & Sharifzadeh, M. Development of a model for analysis of slope stability for circular mode failure using genetic algorithm. *Environ. Earth Sci.* **71**, 1267–1277 (2014).
65. Suman, S., Khan, S., Das, S. & Chand, S. Slope stability analysis using artificial intelligence techniques, Natural Hazards, vol. 84, pp. 727–748, (2016).
66. Armstrong, J. & Collopy, F. The selection of Error measures for Generaliz-ing about forecasting methods: empirical comparisons. *Int. J. Forecast.* **8** (1), 69–80 (1992).

Acknowledgements

The authors extend their appreciation to the Deanship of Scientific Research at King Khalid University for funding this work through large Groups Project under grant number RGP.2/100/45.

Author contributions

Mohammad A. Al-Zubi, Mahmood Ahmad: Conception, Methodology, Investigation, Formal analysis, writing—original draft preparation, software. Shahriar Abdullah, Beenish Jehan Khan, Wajeeha Qamar, Gamil M. S. Abdullah, Sonjoy Paul: Validation, Formal analysis, Visualization. Roberto Alonso González-Lezcano: Investigation, Resources, Supervision, Project Administration, writing—review & editing, N. S. Abd EL-Gawaad, Tariq Ouahbi, and Muhammad Kashif: Validation, Funding acquisition, Software, Investigation, Data curation, writing—review & editing,

Funding

The current work was assisted financially to the Dean of Science and Research at King Khalid University via the Large Group Project under grant number RGP. 2/100/45.

Declarations

Competing interests

The authors declare no competing interests.

Additional information

Correspondence and requests for materials should be addressed to M.A.

Reprints and permissions information is available at www.nature.com/reprints.

Publisher's note Springer Nature remains neutral with regard to jurisdictional claims in published maps and institutional affiliations.